

POLITECNICO DI TORINO

Master's Degree in Communications and Computer
Networks Engineering



Master's Degree Thesis

Optimization strategies for high speed Passive Optical Networks

Supervisors

Prof. Roberto GAUDINO

PhD Student Leonardo MINELLI

Candidate

Ahmed ABDELLATIF

July 2022

Summary

With Cloud Services, Internet of Things (IoT), 5G, 6G and other emerging technologies continuously pushing bandwidth demands, the development of the optical access networks based on Passive Optical Network technology became essential. This has resulted in the industry introducing several generations of PON over the years. Nowadays, XG-PON operates at a speed of 10 Gbits/s in both upstream and downstream. In the years ahead, there would be a shift toward next generation PON (50-GPON G9804.3), which had recently been standardized in 2021 by ITU-T, introducing for the first time, a receiver feed forward equalization (FFE) and Avalanche photodiode receiver (APD-RX). Alternatively, Semiconductor optical amplifier (SOA) and PIN (SOA+PIN) can replace APD.

Several impairments may distort the transmitted signal while operating at high bitrates, some of which originate from the components in use such as bandwidth limitations at the transmitter and at the receiver side, chromatic dispersion and fiber non-linearities along the fiber, quantization noise relative to analog-to-digital converters (ADC), thermal noise due to transimpedance amplifier (TIA), shot noise in APD or SOA ase noise.

The scope of this Thesis is restricted to the analysis of signal-dependent noises in APD-RX and SOA+PIN RX along with the implementation of optimization strategies for detection.

Fig 1 Illustrates the two architectures of the PON receiver considered in this Thesis

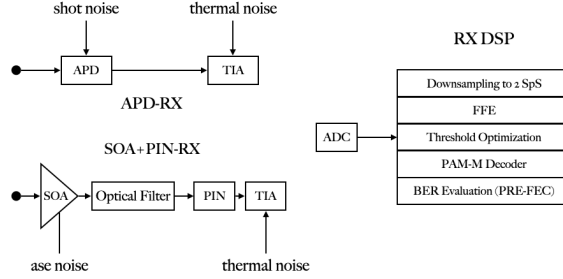


Figure 1: PON Receiver's architectures

At the initial stage, we started by analyzing APD-RX at different values for the extinction ratio and the transmitter's cut off frequency. We investigated both PAM-2 at 50 Gbits/s and PAM-4 at 100 Gbits/s while optimizing the decision thresholds inside a DSP-based FFE. As for PAM-4 only, we also optimize the two internal transmitted levels using a grid search approach.

The results of APD-RX analysis in terms of Optical Path Loss (OPL) as a function of Extinction Ratio (ER) and 3-dB-TX bandwidth are illustrated in Fig.2 and in Fig.3.

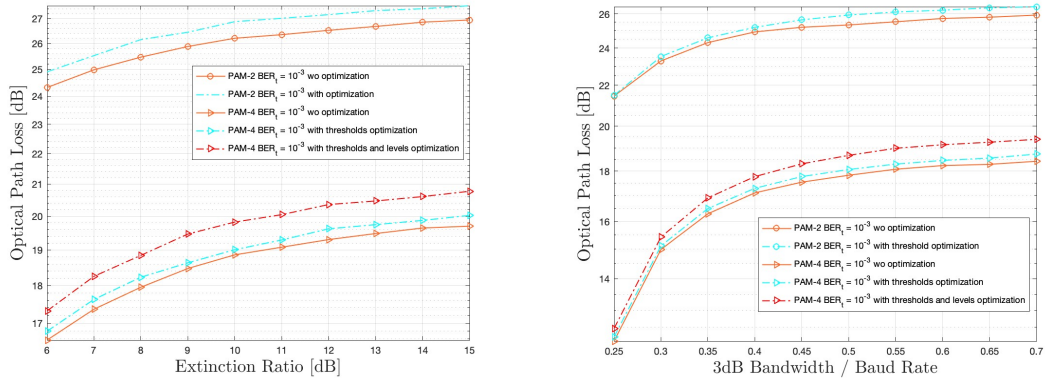


Figure 2: Optical Path Loss (OPL) vs. Extinction Ratio (ER) for APD-RX **Figure 3:** Optical Path Loss (OPL) vs. 3-dB TX bandwidth for APD-RX

We further studied SOA+PIN RX noise at various values of ER, transmitter 3-dB bandwidth and SOA gain. We inspected both PAM-2 and PAM-4 while exploiting the same optimization techniques.

The possible gains in terms of OPL are shown in Fig. 4, in Fig. 5 and in Fig. 6

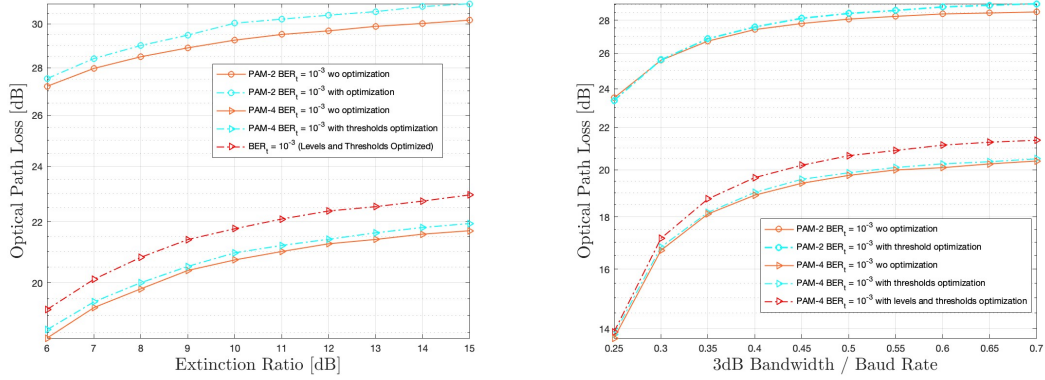


Figure 4: Optical Path Loss (OPL) vs. Extinction Ratio (ER) for SOA+PIN-RX **Figure 5:** Optical Path Loss (OPL) vs. 3-dB TX bandwidth for SOA+PIN-RX

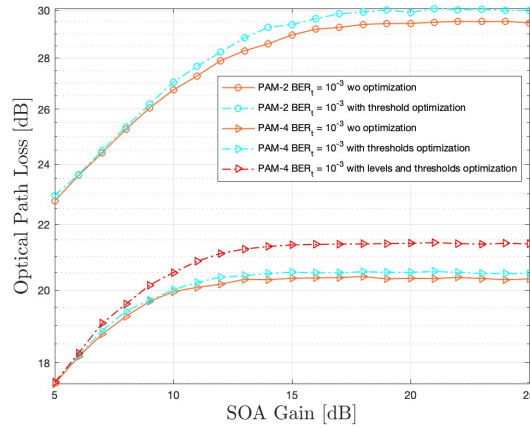


Figure 6: Optical Path Loss (OPL) vs. Semiconductor Optical Amplifier Gain

Finally, considering the results obtained in this thesis as a starting point, we advice using Artificial Neural Network based equalizers for future work related to PAM-4 inner levels optimization instead of using a grid search approach.

Acknowledgements

I would like to thank professor *Roberto Gaudino* for his patience and his kindness in guiding me to accomplish this work. I would also like to acknowledge the tremendous support of *Leonardo Minelli*, PhD student at Poltecnico di Torino.

Finally, I would like to thank everyone who gave me hope through out these years.

Table of Contents

List of Tables	VII
List of Figures	IX
Acronyms	XII
1 Introduction	1
1.1 Brief history of optical communications	2
1.2 Optical communication schemes	3
1.3 Passive optical networks	4
1.3.1 Principle of operation of PON	5
1.4 Modulation schemes	6
1.4.1 PAM-M	7
1.4.2 Analog intensity modulation	7
1.5 Photodetectors	9
1.5.1 PIN Photodiode	9
1.5.2 APD Photodiode	11
1.5.3 Photodetection shot noise	11
1.6 Optical amplifiers	13
1.6.1 Semiconductor Optical Amplifier	13
1.6.2 Amplified Spontaneous Emission noise	14
1.7 Optical filters	16
1.7.1 Super Gaussian Filter	16
1.8 PON Receiver Architectures	18
1.8.1 APD Receiver front-end	18
1.8.2 SOA+PIN Receiver front-end	19
1.9 Problem Identification	20
1.10 Thesis Outline	21

2	Equalization and Optimization Techniques	22
2.1	Equalization	23
2.1.1	FFE	23
2.1.2	LMS and LMF Algorithms	24
2.2	Techniques of optimization	27
2.2.1	Thresholds Optimizer	28
2.2.2	Levels Optimizer	30
2.3	Conclusions	32
3	APD Simulations	34
3.1	Simulation setup	35
3.2	PAM-2 Performance analysis	37
3.2.1	Assessment against various extinction ratios	38
3.2.2	Assessment against 3-dB bandwidth of transmitter	40
3.3	PAM-4 Performance analysis	42
3.3.1	Assessment against various extinction ratios	43
3.3.2	Assessment against 3-dB bandwidth of transmitter	46
3.4	Conclusions	49
4	SOA+PIN Simulations	50
4.1	Simulation setup	51
4.2	PAM-2 Performances analysis	53
4.2.1	Assessment against various extinction ratios	54
4.2.2	Assessment against 3-dB bandwidth of transmitter	56
4.2.3	Assessment against optical amplifier gain	58
4.2.4	Assessment against 3-dB bandwidth of optical filter	59
4.3	PAM-4 Performance analysis	60
4.3.1	Assessment against various extinction ratios	61
4.3.2	Assessment against 3-dB bandwidth of transmitter	64
4.3.3	Assessment against optical amplifier gain	67
4.3.4	Assessment against 3-dB bandwidth of optical filter	68
4.4	Conclusions	69
	Bibliography	70

List of Tables

1.1	TDMA-PON standards [6]	6
1.2	Noises in PON receivers	20
2.1	FFE Parameters	26
2.2	PAM-4 optimum inner levels for APD receiver	30
2.3	PAM-4 optimum inner levels for SOA+PIN receiver	31
3.1	Simulation parameters for the APD receiver	36
3.2	APD shot noise penalty	37
3.3	APD sensitivity enhancement at 9 dB of ER	39
3.4	APD shot noise penalty at f_{3db} of $0.3 R_s$ for PAM-2	40
3.5	APD sensitivity enhancement	41
3.6	APD shot noise penalty for PAM4 vs. PAM-2	42
3.7	APD sensitivity enhancement for PAM-4 after optimizing thresholds for PAM-4	44
3.8	APD sensitivity improvement after optimizing levels and thresholds of PAM-4	45
3.9	APD shot noise penalty at f_{3db} of $0.3 R_s$ for PAM-4	46
3.10	APD sensitivity enhancement for PAM-4 after optimizing thresholds	47
3.11	APD sensitivity enhancement for PAM-4 after optimizing levels and thresholds	48
4.1	Simulation parameters for SOA+PIN receiver	52
4.2	SOA ASE noise penalty	53
4.3	SOA+PIN sensitivity enhancement at 15 dB of ER	55
4.4	SOA ASE noise penalty at f_{3db} of $0.3 R_s$ for PAM-2	56
4.5	SOA+PIN sensitivity enhancement at $f_{3dB,electrical}$ of $0.7 R_s$	57
4.6	SOA+PIN sensitivity enhancement at BER_t of 10^{-3}	58
4.7	SOA+PIN sensitivity enhancement at $f_{3dB,optical}$ of 300 GHz for NRZ	59
4.8	SOA ASE noise penalty for PAM4 vs. PAM-2	60

4.9	SOA+PIN sensitivity enhancement for PAM-4 after optimizing thresholds	62
4.10	SOA+PIN sensitivity improvement for PAM-4 after optimizing levels and thresholds	63
4.11	Bandwidth limitation penalty at $f_{3dB,electrical}$ of 25% of baud rate compared to 70% for PAM-4 while having ase noise	64
4.12	SOA+PIN sensitivity enhancement for PAM-4	65
4.13	SOA+PIN maximum sensitivity enhancement	66
4.14	SOA+PIN sensitivity enhancement at 25 dB of SOA gain for PAM-4	67
4.15	SOA+PIN sensitivity enhancement at $f_{3dB,optical}$ of 300 GHz for PAM-4	68

List of Figures

1	PON Receiver's architectures	ii
2	Optical Path Loss (OPL) vs. Extinction Ratio (ER) for APD-RX	ii
3	Optical Path Loss (OPL) vs. 3-dB TX bandwidth for APD-RX	ii
4	Optical Path Loss (OPL) vs. Extinction Ratio (ER) for SOA+PIN-RX	iii
5	Optical Path Loss (OPL) vs. 3-dB TX bandwidth for SOA+PIN-RX	iii
6	Optical Path Loss (OPL) vs. Semiconductor Optical Amplifier Gain	iii
1.1	Optical semaphore telegraph [2]	2
1.2	Illustration of IM-DD receiver	3
1.3	Illustration of coherent receiver	3
1.4	Illustration of Passive Optical Networks	4
1.5	TDMA-PON with a WDM feature	5
1.6	PAM-2 and PAM-4 constellations in I-Q plane	7
1.7	Illustration of Directly Modulated Laser (DML)	8
1.8	PIN physical structure [9]	9
1.9	PIN responsivity as a function of wavelength [9]	10
1.10	APD physical structure [9]	11
1.11	Illustration of APD with shot noise	12
1.12	SOA structure [13]	13
1.13	Stimulated Emission process [3]	14
1.14	Illustration of SOA with ASE noise	15
1.15	Magnitude squared of the optical filter frequency response $ H(f) ^2$ plot at different filter orders	16
1.16	Illustration of a SOA followed by an optical filter	17
1.17	Block-diagram of APD Receiver front-end	18
1.18	Block-diagram of SOA+PIN Receiver front-end	19
1.19	Eye-diagram of PAM-2 after noise loading	20
1.20	Eye-diagram of PAM-4 after noise loading	20
2.1	Linear equalizer structure: where $r[k]$ is the input sequence, $d[k]$ is the training sequence (also referred to as the desired response), $y[k]$ is the output sequence, $w_n[k]$ are the adjustable equalizer taps	23

2.2	Eye-diagram of PAM-2 post-FFE	26
2.3	Eye-diagram of PAM-4 post-FFE	26
2.4	Eye-diagram of PAM-2 showing the degree of freedom for optimization	27
2.5	Eye-diagram of PAM-4 showing the degrees of freedom for optimization	27
2.6	PAM-2 V_{Th} vs BER curve at ER of 9 dB and OPL of 27 dB	28
2.7	PAM-4 $V_{1,2,3}$ vs BER curve at ER of 6 dB and OPL of 17 dB	28
2.8	Threshold Optimizer building-blocks	29
2.9	$V_{1,Opt}$ for NRZ at ER of 9 dB, $f_{3,dB}$ of 35 GHz and OPL of 27 dB	29
2.10	$V_{1,2,3,Opt}$ for PAM-4 at ER of 6 dB, $f_{3,dB}$ of 35 GHz and OPL of 17 dB	29
2.11	Contour plot of PAM4 inner levels for APD at ER of 6 dB, $f_{3dB,electrical}$ of 35 GHz and OPL of 17 dB	30
2.12	Contour plot of PAM4 inner levels for SOA+PIN at ER of 9 dB, $f_{3dB,electrical}$ of 35 GHz and OPL of 21 dB	31
2.13	Eye-diagram of PAM-2 with threshold optimization at ER of 9 dB and OPL of 21 dB	32
2.14	Eye-diagram of PAM-4 with threshold optimization at ER of 6 dB and OPL of 17 dB	33
2.15	Eye-diagram of PAM-4 with threshold and levels optimization at ER of 6 dB and OPL of 17 dB	33
3.1	APD Simulation Setup	35
3.2	ROP vs. BER curve for NRZ at ER of 9 dB and $f_{3dB,electrical}$ of 35 GHz	37
3.3	ER vs. OPL curves with and without shot noise for NRZ	38
3.4	ER vs. OPL curve with and without threshold optimization relevant to NRZ at $f_{3dB,electrical}$ of 35 GHz	39
3.5	$f_{3dB,electrical}$ vs. OPL curve with and without shot noise for NRZ at BER_t of 10^{-2}	40
3.6	$f_{3dB,electrical}$ vs. OPL curve with and without threshold optimization relevant to NRZ at ER of 9 dB	41
3.7	ROP vs. BER curve for PAM4 at ER of 9 dB and $f_{3dB,electrical}$ of 35 GHz	42
3.8	ER vs. OPL curves with and without shot noise for PAM-4	43
3.9	ER vs. OPL curve with and without thresholds optimization relevant to PAM-4 at $f_{3dB,electrical}$ of 35 GHz	44
3.10	ER vs. OPL curve with and without thresholds and levels optimization relevant to PAM-4 at $f_{3dB,electrical}$ of 35 GHz	45
3.11	$f_{3dB,electrical}$ vs. OPL curve with and without shot noise for PAM-4	46
3.12	$f_{3dB,electrical}$ vs. OPL curve with and without thresholds optimization relevant to PAM-4 at ER of 9 dB	47

3.13	$f_{3dB,electrical}$ vs OPL curves with and without threshold and levels optimization relevant to PAM-4 at ER of 9 dB	48
4.1	SOA+PIN Simulation Setup	51
4.2	ROP vs BER curve for NRZ at ER of 9 dB and $f_{3dB,electrical}$ of 35 GHz	53
4.3	ER vs OPL curve with and without ASE noise for NRZ	54
4.4	ER vs OPL curve with and without threshold optimization relevant to NRZ at $f_{3dB,electrical}$ of 35 GHz	55
4.5	$f_{3dB,electrical}$ vs OPL curve with and without ASE noise for NRZ at BER_t of 10^{-2}	56
4.6	$f_{3dB,electrical}$ vs OPL curve with and without threshold optimization relevant to NRZ at ER of 9 dB	57
4.7	SOA gain vs OPL curve with and without threshold optimization for NRZ	58
4.8	$f_{3dB,optical}$ vs OPL with and without threshold optimization relative to NRZ	59
4.9	ROP vs BER for PAM4 at ER of 9 dB and $f_{3dB,electrical}$ of 35 GHz .	60
4.10	ER vs OPL curve with and without ase noise for PAM-4	61
4.11	ER vs OPL curve with and without threshold optimization for PAM-4 at nominal inner levels	62
4.12	ER vs OPL curve with and without threshold optimization relevant to PAM-4 at optimized inner levels	63
4.13	$f_{3dB,electrical}$ vs OPL curve with and without ASE noise for PAM-4 .	64
4.14	$f_{3dB,electrical}$ vs OPL curve with and without threshold and levels optimization relevant to PAM-4 at ER of 9 dB	65
4.15	$f_{3dB,electrical}$ vs OPL curve with and without threshold and levels optimization relevant to PAM-4 at ER of 9 dB	66
4.16	SOA gain vs OPL curve with and without threshold optimization for PAM-4	67
4.17	$f_{3dB,optical}$ vs OPL curve with and without threshold optimization relevant to PAM-4	68

Acronyms

ADC

Analog to Digital Converter

AWGN

Additive White Gaussian Noise

APD

Avalanche Photodiode

BER

Bit Error Rate

DAC

Digital to Analog Converter

DSP

Digital Signal Processing

FFE

Feedforward Equalizer

FTTH

Fiber To The Home

IM

Intensity Modulator

IRND

Input Referred Noise Density

ISI

Inter-Symbol Interference

MSE

Mean Square Error

NRZ

Non Return to Zero

OPL

Optical Path Loss

PAM

Pulse Amplitude Modulation

PON

Passive Optical Network

PSD

Power Spectral Density

SOA

Semiconductor Optical Amplifier

Chapter 1

Introduction

Over the past years, there had been huge technological advancements in the field of optical communications. Fibers are currently deployed not only in long-haul communications as core networks but also in mid-reach and short-reach applications such as Data Center Interconnect (DCI) that connects data centers together and access networks which connect subscribers to service providers. Nowadays, Fiber to the home (FTTH) technology is evolving to meet the demand for ultra-fast access networks (50Gbps/ λ) and beyond. However, it becomes necessary to counteract several impairments using either pre-processing and/or post-processing (equalization) to compensate physical layer impairments.

This Thesis will specifically cover FTTH-PON deployed in IM/DD scheme. We will mainly deal with different noises impairments exploiting Digital Signal Processing (DSP) optimization techniques

This introductory chapter is divided into the following Sections :

- **Section 1.1** : Brief history of optical communications.
- **Section 1.2** : Brief introduction of optical communication schemes.
- **Section 1.3** : Introducing Passive Optical Networks
- **Section 1.4** : Modulation schemes used in PON
- **Section 1.5** : Photo-detectors and photo-detection noise
- **Section 1.6** : Introducing optical amplifiers and optical filters used in PON
- **Section 1.8** : Problem identification at PON receivers front-end

1.1 Brief history of optical communications

Optical communications date back to the 1790s, to the optical semaphore telegraph invented by French inventor Claude Chappe [1].



Figure 1.1: Optical semaphore telegraph [2]

In **1880**, Alexander Graham Bell invented the photophone carrying audio signals through air. This invention was never materialized but it triggered what is referred to now as free space optics FSO.

In **1954**, Abraham Van Heel covered a bare glass with coating making it possible to transmit light through fiber without any leakage.

In **1980**, Bells Labs proposes first fiber transatlantic cable (TAT-8) using single mode fiber and transmitting at speed of 565 Mbps over 2 pair fibers.

In **1984**, Microwave communications Inc. install a link between New York and Washington operating at 400 Mbps.

In **1992**, It was possible to use C-band (1550 nm) band where fiber attenuation goes down to 0.2 dB/Km and Erbium Doped Fiber Amplifiers (EDFA) operate.

By **1995**, Wavelength Division Multiplexing (WDM) was developed making it possible to transmit over multiple wavelengths down the same fiber.

In **2006-2008**, The Coherent systems were developed and became commercially available, running at 40 Gbps based on QPSK modulation.

In **2010-2013**, more complex formats such as PM-QAM were used for coherent systems as well as advanced DSP and FECs.

By **2020**, The Spatial Division Multiplexing (SDM) revolution starts, Multi-core fiber will be applied for longhaul.

1.2 Optical communication schemes

In this Section, we will classify the optical system based on its photo-detection technique.

- **Intensity Modulation with Direct Detection (IM-DD):** It is the simplest and most used optical communication scheme where the light emitted is the only one degree of freedom used for conveying information. The polarization and phase of the optical signal are not recovered at receiver side [3].

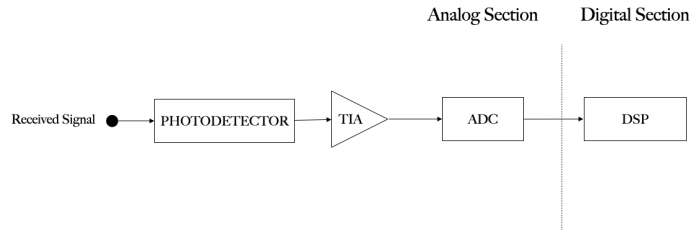


Figure 1.2: Illustration of IM-DD receiver

In IM-DD, since the transmitted information is associated only with the intensity variation of the field, the information is recovered using only a single photo-diode to directly detect the envelope of the field.

- **Coherent:** It is a more sophisticated scheme where optical signal is modulated with information using phase, frequency and amplitude. Moreover, at receiving-end, detection by interference takes place using a local oscillator, polarization beam splitters and hybrid devices.

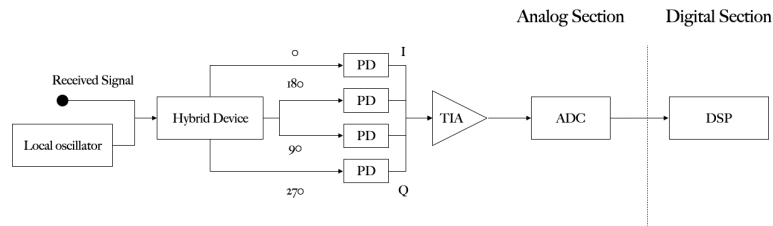


Figure 1.3: Illustration of coherent receiver

There are two approaches for signal detection in coherent receivers, the first approach is called the *heterodyne method* where the incoming signal is combined with a reference wave of a LO (Laser) that produces another wave at an intermediate frequency. The second approach is the *homodyne method* which is similar to the previous method except that the LO has the same frequency and phase as the incoming optical signal. After that, the signal passes through a hybrid device to extract its four field components. Finally, direct detection takes place.

Coherent scheme is usually deployed in long-haul transmission because it allows using more advanced modulations such as Quadrature Amplitude Modulation (QAM-M). Therefore, it can achieve higher bitrates. It can also be used in short-reach applications, but it is not as favored as IM-DD because it is very expensive. This Thesis focuses only on short-reach applications that use IM/DD.

1.3 Passive optical networks

In this Section, we will introduce Passive Optical Networks (PONs) as an application of IMDD, we will highlight its main components and its principle of operation. PON is a cost-efficient technology that exploits a shared optical infrastructure to provide connectivity. The main application of PON is FTTH illustrated in Fig. 1.4. However, as PON technologies have improved, PON application scope has extended to new applications such as 5G front-haul: connecting 5G Baseband Unit (BBU) to the Remote Radio Head (RRH)[4]. Similarly to FTTH, signals from 5G base-band units are distributed to multiple remote radio units [5].

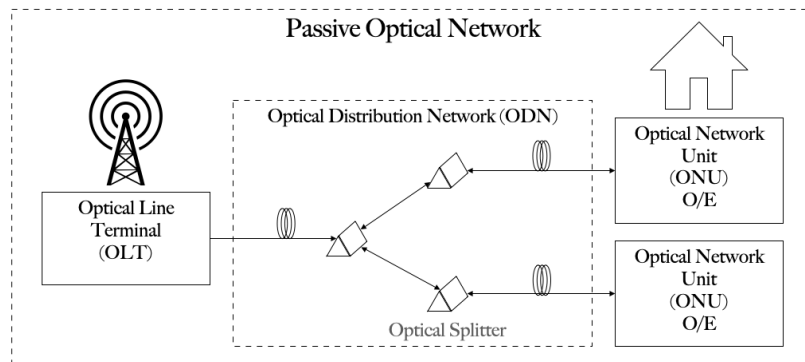


Figure 1.4: Illustration of Passive Optical Networks

Passive optical networks consist of :

- **Optical line terminal (OLT):** It is the terminal where signal is generated. it could either be a 4G/5G base-band units or a transmitter at the service provider.
- **Optical distribution network (ODN):** It is distribution network which contains only passive devices such as splitters. typical splitting ratios are 1:32, 1:64 or even 1:128 at an affordable cost of insertion loss.
- **Optical network unit (ONU):** It is a simple optical modem / receiver that aims to carry out O/E conversion and the DSP that follows at the receiving end.

1.3.1 Principle of operation of PON

:

The optical signal in passive optical network is distributed to multiple branches by means of optical passive devices called optical splitters followed by WDM multiplexers and demultiplexers to enable simultaneous transmission of upstream and downstream signals on the same fiber.

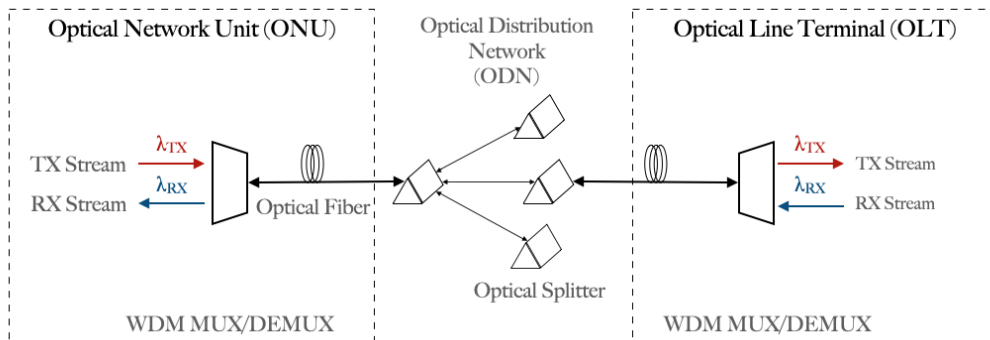


Figure 1.5: TDMA-PON with a WDM feature

The vast majority of PON standards uses Time Division Multiple Access (TDMA) in upstream to prevent collision of signals sent by many ONUs at the splitter. Each ONU in a TDMA-PON must send its data within a dedicated time slot.

GPON and EPON are the currently deployed standards but others have already been published, These standards have been developed over the years to meet the demand for higher capacities. In Fig 1.1, we report some of these standards.

Name	Standards	Characteristics	
		Upstream	Downstream
GPON	ITU-T G984.x	2.5 Gbps	1.25 Gbps
EPON	IEEE 802.3ah	1 Gbps	1 Gbps
XG-PON	ITU-T G987.x	10 Gbps	2.5 Gbps
XGS-PON	ITU-T G9807.1	10 Gbps	10 Gbps
Higher Speed	ITU-T G.9804.3	Under-definition	50 Gbps

Table 1.1: TDMA-PON standards [6]

Most recently in 2021, ITU-T had standardized Higher Speed PON which will provide symmetric speeds of 50 Gbits/s/λ. However, we will have to deal with several challenges at the physical layer, operating at such high bitrates: bandwidth limitations, fiber chromatic dispersion (CD), non-linearities and photo-detection noises.

1.4 Modulation schemes

Most currently adopted Passive Optical Networks employ IM/DD scheme for techno-economic reasons and complexity reduction at ONU. In this Section, NRZ and Multi-Level PAM modulations are discussed as they are used in IM/DD - PONs.

To access the performance when using a specific format, several metrics are exploited.

- **Bit error rate** : BER is the number of error per unit time. For a given signal to noise ratio (SNR), BER increases as the cardinality of modulation increases.
- **Spectral efficiency** : Spectrum efficiency describes the amount of data transmitted over a given bandwidth.

$$\eta_B = \frac{R_{bit}}{B} = \frac{2 \log_2 M}{N_d} \quad (1.1)$$

where R_{bit} is the bit rate, B is the occupied bandwidth, M is the constellation order, N_d is the number of dimensions.

1.4.1 PAM-M

PAM-2 and PAM-4 are the most used digital base-band modulation techniques for IM/DD. Alphabet of PAM-M can be represented as $A = [(2m - M - 1)\Delta]_{m=1}^M$ [7] where M is the order of modulation and Δ is real number. Therefore, PAM-M symbols are purely real. In higher speed PON at the moment of carrying out this work PAM-2 has already been introduced in the standard for downstream and PAM-4 is in research.

Typical examples of PAM-2 and PAM-4 scatter-diagrams are illustrated in Fig.1.6

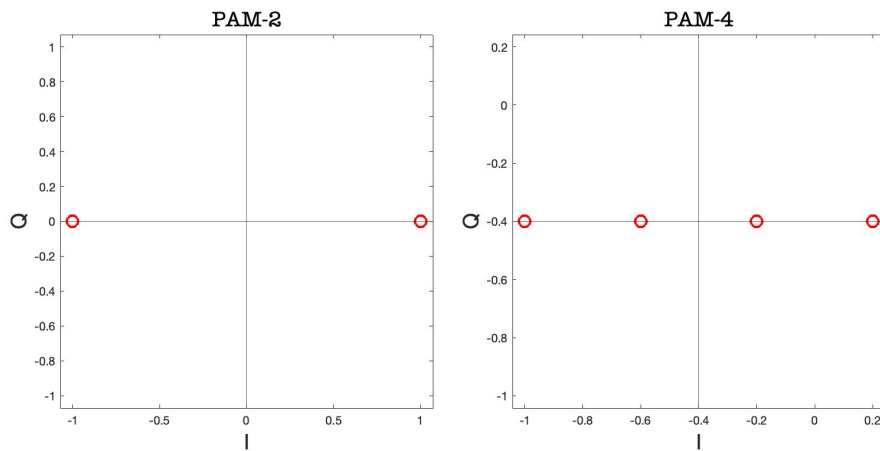


Figure 1.6: PAM-2 and PAM-4 constellations in I-Q plane

1.4.2 Analog intensity modulation

Intensity modulation is the technique where the intensity of light is modulated with the analog signal directly or by means of an external modulator. The work done in this Thesis assumes an ideal and linear Directly Modulated Laser (DML) to employ multi-level formats such as PAM.

DML can be modelled as an affine transformation. It assumes that the input bias current exceeds the laser threshold for it to operate. However, in practice the output signal of semi-conductor DML is distorted due to the change in carrier density in the active layer of the laser[8]. This non-linear effect will not be considered in this Thesis.

Typical illustration of DML is in Fig.1.7.

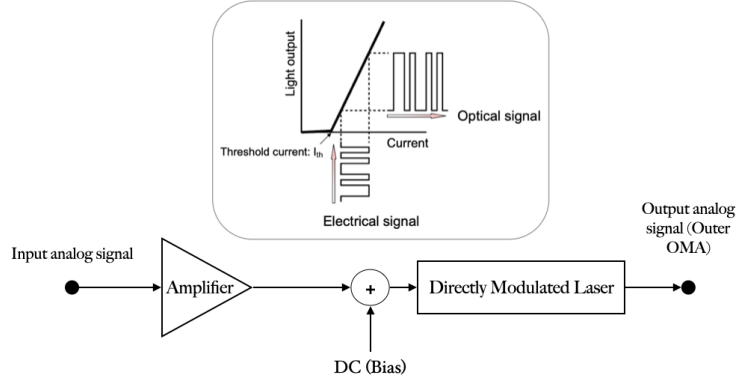


Figure 1.7: Illustration of Directly Modulated Laser (DML)

The output optical signal of DML can be characterized in terms of *extinction ratio* which is the ratio between the uppermost level and the lowest one.

$$ER = \frac{P_{(M-1)}}{P_0} \quad (1.2)$$

The average output power is :

$$\bar{P} = \frac{P_{(M-1)} + P_0}{2} \quad (1.3)$$

Given a specific average output power and a specific extinction ratio, the two power levels can be computed using Eq. 1.2 and Eq. 1.3 then in order to realize it using a DML, the gain and bias have to be evaluated using the linear transformation in the following equations.

$$Tx_{(M-1)}G + b = P_{(M-1)} \quad (1.4)$$

$$Tx_0G + b = P_0 \quad (1.5)$$

- ER is the extinction ratio
- G is the laser gain
- Tx_n is the PAM-M symbol corresponding to n alphabet
- P_n is the power corresponding to n level
- b is the DC component

1.5 Photodetectors

Once the optical signal is modulated, as it propagates through the fiber it experiences attenuation and some linear and non-linear effects due to the fiber and as it arrives at the receiver, an O/E conversion is processed using a photodetector. Ideally, each photon of the received optical signal is translated by the photodiode into at least one free electron. In this Section, we will discuss the *PIN photodiode* and the *Avalanche photodiode* used in PON receivers.

1.5.1 PIN Photodiode

PIN photodetector is a semiconductor device capable of operating at a very high bitrates. It consists of a p-n junction separated by a very lightly n-doped depletion region and a large reverse bias voltage applied across its terminals.

Fig. 1.8 illustrates the physical structure of the PIN.

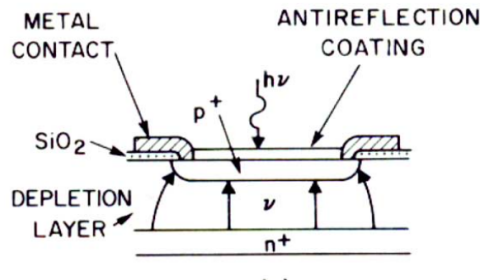


Figure 1.8: PIN physical structure [9]

In normal operating conditions, whenever an incident photon impinges on the surface of the photodetector with an energy exceeding band-gap energy of the material, an electron is excited from valence to conduction band, thereby generating a free electron hole pair. Under the influence of an external electric field, electrons and holes are swept across the drift (depletion) region which will give rise to a current flow.

Given a received electric field expression:

$$E(t) = [E_{Ix}(t) + jE_{Qx}(t)]\hat{x} + [E_{Iy}(t) + jE_{Qy}(t)]\hat{y} \quad (1.6)$$

The photodiode generates photocurrent proportional to the electric field multiplied by its conjugate.

$$I(t) \propto E(t) * E(t)^* \quad (1.7)$$

By substituting $E(t)$ by its four components, we get :

$$I(t) \propto |E_{Ix}(t)|^2 + |E_{Qx}(t)|^2 + |E_{Iy}(t)|^2 + |E_{Qy}(t)|^2 \propto P(t) \quad (1.8)$$

Therefore, the generated photocurrent is the instantaneous power multiplied by a coefficient of proportionality termed as the responsivity of the photodiode.

$$I_{PIN}(t) = RP(t) \quad (1.9)$$

The responsivity of the photodiode is the ratio between the generated electrons (photocurrent) to the number of incident photons (optical power). In practical photodiodes, not every incoming photon is able to create an electron. Thus, the responsivity of a photodiode is never equal to one. It is also dependent on the wavelength of operation which depends intrinsically on the photodetector material. In Fig. 1.9, we show PIN responsivity for different materials as a function of wavelength (λ).

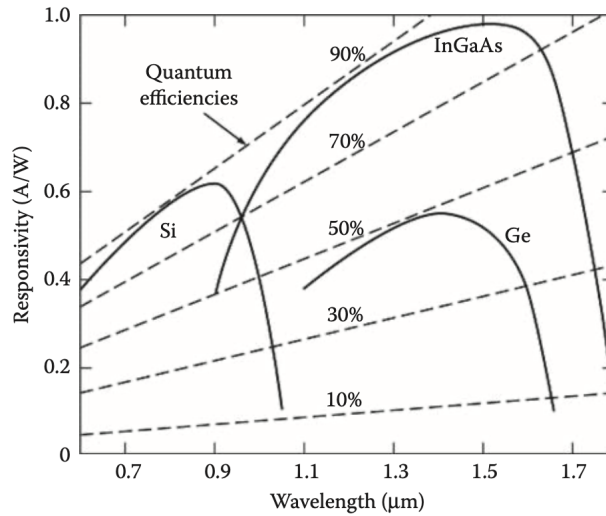


Figure 1.9: PIN responsivity as a function of wavelength [9]

We can notice variations in terms of the available bandwidth of the photodetectors of different materials.

1.5.2 APD Photodiode

Avalanche photodiode is similar to PIN with the exception of providing an intrinsic gain through a process called repeated **electron ionization** (avalanche process).

The avalanche process is a multiplication process where the electrons get accelerated in a high electric field region which is exclusively present in the APD structure. As the electrons get accelerated, the accelerated electrons ionize the atoms and the whole process becomes iterative in a cascading fashion. [3]. The APD structure is shown in Fig. 1.10.

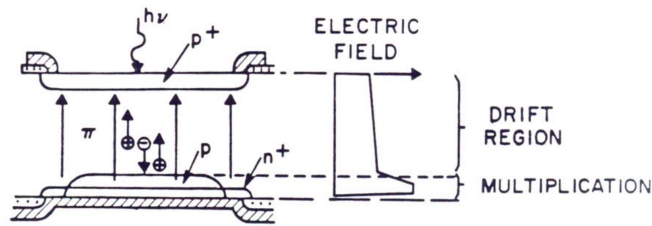


Figure 1.10: APD physical structure [9]

The photocurrent expression for the APD also exhibits dependency on the instantaneous received power, multiplied by an APD gain (M).

$$I_{APD}(t) = MRP(t) \quad (1.10)$$

The main advantage of the APD is that it has a greater level of sensitivity compared to PIN. The avalanche process increases the gain of the diode many times, providing much higher sensitivity. However, there are disadvantages, including:

- High vulnerability to temperature changes.
- Requiring higher reverse bias compared to PIN.
- There is always noise associated to APD relevant to the statistical nature of the avalanche process that is called *excess noise*, as discussed in the next Section.

1.5.3 Photodetection shot noise

The only notable noise affecting the system performance is the noise related to the quantum nature of photons[3]. The random times of arrival of the photons that hit the photodetector generate noise that is referred to as *Shot noise*.

Shot noise is often regarded as an additive white Gaussian noise (AWGN) that is additive to the generated photo-current.

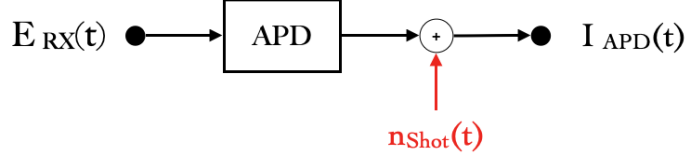


Figure 1.11: Illustration of APD with shot noise

Considering an APD, the expression of the generated photo-current is :

$$I_{APD}(t) = MRP(t) + n_{shot}(t) \quad (1.11)$$

APD shot noise Power Spectral Density (PSD) is defined as :

$$N_{0-Shot}(t) = 2qFM^2RP_{rx}(t) \quad (1.12)$$

where,

- q is electron charge = 1.6^{-19} in [coulomb]
- F is the dimensionless excess noise figure
- M is the linear APD gain
- R is the responsivity [A/W]
- $P_{rx}(t)$ is the instantaneous received power in [watt]

The excess noise is due to the unequal multiplication of carriers within the APD multiplication region. It is quantified by the excess noise factor (F) expressed as:

$$F = k_F M + (1 - k_F) \left(2 - \frac{1}{M} \right) \quad (1.13)$$

Where M is the APD gain and k_F is the ionization factor.

The Excess noise factor will always be greater than one for the APD.

Shot noise variance is :

$$\sigma_{Shot}^2(t) = N_{0-Shot}(t)B \quad (1.14)$$

where B is the unilateral noise bandwidth in [Hz].

According to Eq. 1.14, the variance *APD shot noise* depends on the *instantaneous received optical power*. The shot noise impact on the PAM-M levels will be the main focus of this Thesis.

1.6 Optical amplifiers

Optical amplifiers are quantum systems that receive an optical input signal (Gaussian beam) and generates an optical output signal with higher power. The amplification process occurs in the *active region* of the amplifier after applying a proper external pumping. [10]. There are two common type of optical amplifiers represented by *Erbium doped fiber amplifiers* (EDFAs) and *Semiconductor Optical Amplifier* (SOA). EDFAs are advantageous for what concerns noise figure and distortion ($F_{n-EDFA} = 4$ dB while SOA $F_{n-SOA} = 5 - 8$ dB[11]). However, EDFAs are not suitable if the active region is required to be in an integrated device.

In this Section, we will discuss SOA in details as it is considered as a key option in new generation PON due to a potentially lower cost.

1.6.1 Semiconductor Optical Amplifier

SOA comes in the form of fiber-pigtailed components with an integrated active region. It can operate at wavelengths of 1310, 1400, 1500 and 1600 and generate gains up to 30 dB [12]. There are two categories of SOA, *Fabry-Perot Laser Amplifier* (FPLA) and *Traveling-Wave Semiconductor Laser Amplifier* (TWSLA). SOA physical structure is shown in Fig. 1.12.

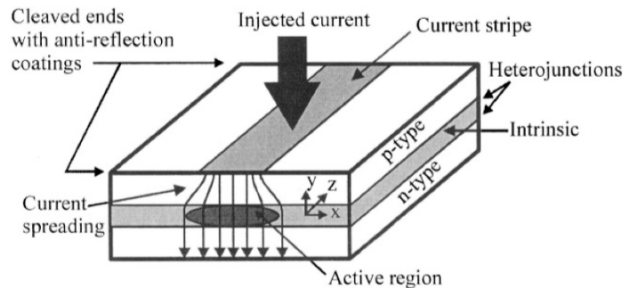


Figure 1.12: SOA structure [13]

For instance, in FPLAs, the signal experiences reflections inside the cavity to be amplified before it is allowed to pass through the back-facet. Whereas, the signal in TWSLA is amplified by a single passage through the active region [14]. TWSLA is usually characterized by having cleaved facets with very small reflectivity or even without reflective facets. We will consider in this Thesis TWSLA with no reflective facets so that SOA non-linear effects are discarded.

Principle of operation of SOA :

Applying an electric current (pump) excites some electrons in the active region of the amplifier and as the light (exciting photons) travels through it, this causes some of these electrons to lose their extra energy in a form of coherent photons that matches the initial ones. This phenomenon is called *stimulated emission*. It is the phenomenon by which the optical signal is amplified. Fig. 1.13 shows an illustration of this process.

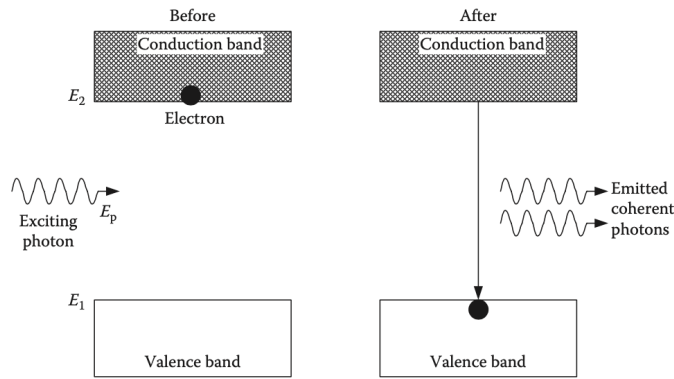


Figure 1.13: Stimulated Emission process [3]

In addition to the stimulated emission, there is another phenomenon that takes place due to the spontaneously emitted photons. It is termed as *spontaneous emission*.

1.6.2 Amplified Spontaneous Emission noise

Since the spontaneously emitted photons generated in the active region of the amplifier are random in phase and direction, they generate noise within the signal's bandwidth. This noise is quantified by Spontaneous-emission factor (n_{sp}).

Amplified Spontaneous Emission noise can be regarded as an additive white Gaussian noise (AWGN) that is added to the optical field due to the optical amplifier.

The received signal can be expressed as (neglecting any phase modulation) :

$$E_{RX}(t) = \sqrt{P_{RX}(t)} \quad (1.15)$$

In Fig. 1.14 SOA is illustrated in the form of a block-diagram.

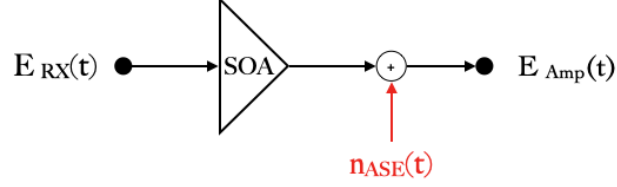


Figure 1.14: Illustration of SOA with ASE noise

According to the illustration above:

$$E_{Amp}(t) = \sqrt{G}E_{RX}(t) + n_{ASE}(t) \quad (1.16)$$

where ASE noise components are expressed in the following equation :

$$n_{ASE}(t) = n_I(t) + jn_Q(t) \quad (1.17)$$

The PSD of the ASE noise is defined as :

$$N_0 = hf_0(G - 1)\frac{F}{2} \quad (1.18)$$

where,

- h is Planck constant = 6.62×10^{-34} [joule/Hz]
- f_0 is the operational frequency in [Hz]
- G is the gain
- F is ASE noise figure and is equal to $2n_{sp}$.

ASE noise variance is :

$$\sigma_{ASE}^2 = N_0B \quad (1.19)$$

where B is the optical unilateral noise bandwidth in [Hz]

It can be noticed that ASE noise PSD exhibits dependency on the amplifier gain, noise figure and wavelength of operation. As an illustration, the noise generated by a SOA operating in O-band ($f_0 = 228.85$ THz) is higher compared to another operating in C-band ($f_0 = 193.40$ THz).

1.7 Optical filters

Optical filters are passive devices used in optical communications to restrict the signal to the spectral band of interest and are possibly made of alternated thin films of materials with different refractive indices or with several other technologies. In this Section, we will discuss the optical filter and its implementation in SOA+PIN receiver.

In PON, optical band-pass filters are often placed after SOA or APD. They are characterized by having very large bandwidth due to the manufacturing process and are often synthesized as **Super Gaussian Filters**

1.7.1 Super Gaussian Filter

Super Gaussian filter (SGF) is a filter whose impulse response is an approximation to a Gaussian function. In Fig. 1.15 we plot the magnitude square of the frequency response of the optical filter: showing $f_{3dB,optical}$ adopted in this Thesis.

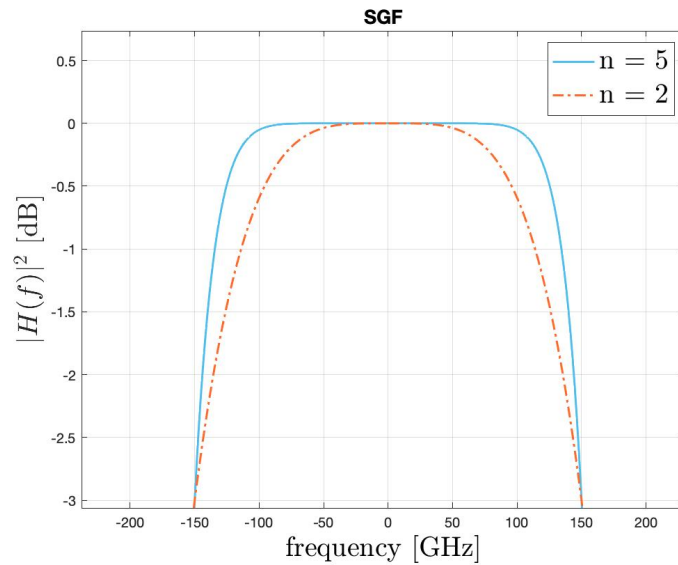


Figure 1.15: Magnitude squared of the optical filter frequency response $|H(f)|^2$ plot at different filter orders

We can notice that increasing the filter order increases the sharpness of the cut-off.

Mathematically, a Gaussian filter modifies the input signal by convolution with a Gaussian function: this transformation is also known as the Weierstrass transform[15]

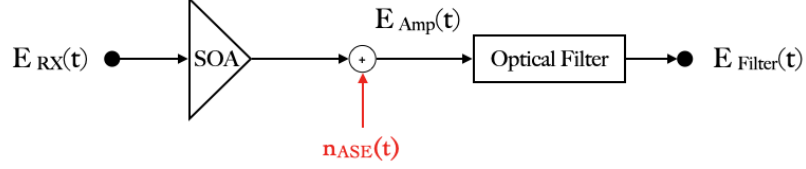


Figure 1.16: Illustration of a SOA followed by an optical filter

The signal at the output of the SOA can be expressed as :

$$E_{Amp}(t) = [\sqrt{G}E_{Ix}(t) + (n_{Ix}(t) + jn_{Qx}(t))]\hat{x} + (n_{Iy}(t) + jn_{Qy}(t))\hat{y} \quad (1.20)$$

where $n(t)$ represent the four ASE noise components

$$E_{Filter}(t) = [E_{x-Amp}(t) * h_x(t)]\hat{x} + [E_{y-Amp}(t) * h_y(t)]\hat{y} \quad (1.21)$$

where $h_x(t)$ and $h_y(t)$ are the optical filter impulse response in x and y polarization.

1.8 PON Receiver Architectures

In all communication systems, identification of noise sources and its nature is fundamental as it might enormously distort the signal. As previously introduced in PON, there are two different receiver architectures:

- Avalanche Photodiode Receiver
- Semiconductor Optical Amplifier + PIN Receiver

In this Section, we will identify the noise sources in each of the two PON receivers.

1.8.1 APD Receiver front-end

In an APD receiver, APDs and Trans-Impedance Amplifiers (TIAs) play vital roles in the conversion processes. However, the noise associated to each of them has different statistical nature. Thus, it has to be studied. In Fig. 1.17, a block-diagram of APD-RX front-end is illustrated.

The two significant noise sources affecting our system performance are :

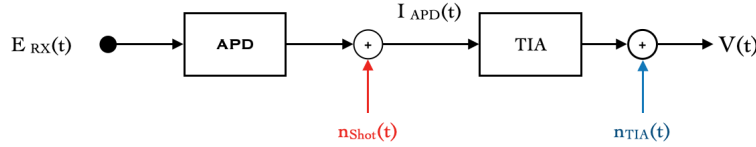


Figure 1.17: Block-diagram of APD Receiver front-end

- **APD Shot noise** $\sim \mathcal{N}(0, \sigma_{Shot}^2(t))$ which is modelled as WGN with variance

$$\sigma_{Shot}^2(t) = 2qFM^2RP_{rx}(t)B \quad (1.22)$$

- **TIA Thermal noise** : TIA noise is a thermal noise added by Trans-Impedance Amplifiers (TIA) due to thermal fluctuations of electrons. It can also modelled as Gaussian distribution with variance

$$\sigma_{th}^2 = (IRND)^2B = N_0B \quad (1.23)$$

where $IRND$ is Input-Referred Noise Density [A/\sqrt{Hz}] and B is the unilateral noise bandwidth in [Hz]

Since APD shot noise and TIA thermal noise are mutually disjoint, the equivalent noise n_{eq} can be modelled as a WGN with time-dependent variance σ_{eq-APD}^2 as :

$$\sigma_{eq-APD}^2(t) = \sigma_{th}^2 + \sigma_{shot}^2(t) \quad (1.24)$$

According to Eq. 1.24, the output signal will be affected by an unbalanced distribution due to shot noise.

1.8.2 SOA+PIN Receiver front-end

In a SOA+PIN receiver front-end, the received signal experiences additive noises due to semiconductor optical amplifiers (SOAs) and Trans-Impedance Amplifiers (TIAs). The evolution of the signal is described in Fig. 1.18.

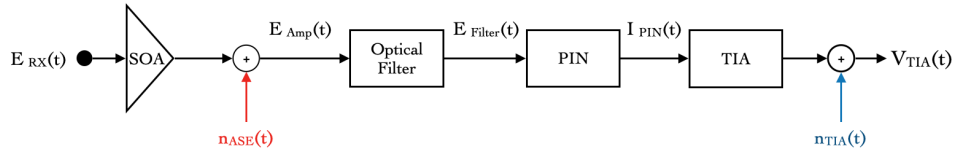


Figure 1.18: Block-diagram of SOA+PIN Receiver front-end

The two noises affecting the signal in SOA+PIN-RX are :

- **SOA ASE noise** $\sim \mathcal{N}(0, \sigma_{ASE}^2(t))$ which is modelled as WGN with variance

$$\sigma_{ASE}^2(t) = hf_0(G-1)\frac{F}{2}B \quad (1.25)$$

- **TIA Thermal noise** $\sim \mathcal{N}(0, \sigma_{TIA}^2)$ discussed in Sec. 1.8.1

By considering SOA ASE noise and TIA thermal noise, the equivalent noise $\sigma_{eq-SOA+PIN}^2$ can also be modelled as a WGN with time-dependent variance :

$$\sigma_{eq}^2(t) = \sigma_{th}^2 + \sigma_{ASE}^2(t) \quad (1.26)$$

1.9 Problem Identification

After studying the physics behind each element in PON receivers, we summarize the noises associated to each element that leads to BER deterioration in Tab. 1.2.

	Associated noise	Nature
APD	excess and shot noise	asymmetric
TIA	thermal noise	symmetric
SOA	ASE noise	asymmetric

Table 1.2: Noises in PON receivers

Typical examples of PAM-2 and PAM-4 signals after noise loading are in Fig.1.19 and Fig.1.20.

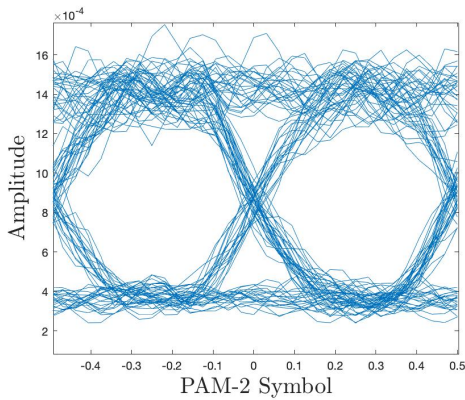


Figure 1.19: Eye-diagram of PAM-2 after noise loading

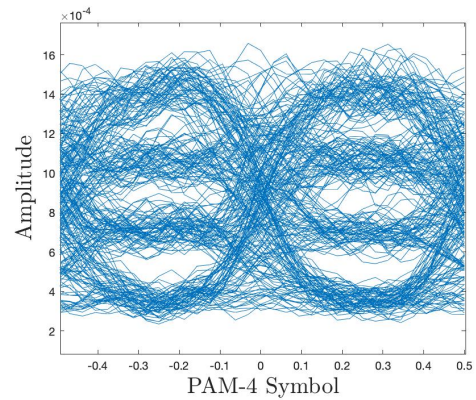


Figure 1.20: Eye-diagram of PAM-4 after noise loading

The scope of this Thesis is limited to mitigating the effect of the asymmetric noises associated to SOA and APD in the following conditions :

- **Bandwidth limitations:** There are many components that can introduce bandwidth limitations such as the electrical filter, the optical filters. Thus, we will analyze the effect of the asymmetric noise while introducing bandwidth limitations.
- **Extinction ratios:** in the case of an asymmetric noise, a possible enhancement could be achieved as the ratio between the most upper and most lower levels increases. Hence, it is important to analyze the system for different ER.

1.10 Thesis Outline

This thesis is subdivided into the following chapters :

- **Chapter 2** : We will introduce post-equalization and optimization techniques to deal with the problem of signal-dependent noises.
- **Chapter 3** : We will simulate the performance of the APD receivers in presence of shot noise and while applying the optimization techniques.
- **Chapter 4** : We will further simulate the performance of SOA+PIN receivers in presence of ase noise and while applying the same optimization techniques.
- **Chapter 5** : We will discuss possible suggestions for the future work related to the topic of optimization.

Chapter 2

Equalization and Optimization Techniques

Up till now, we had identified the problem related to both receivers architecture. (APD-based and SOA+PIN based). In this Chapter, we will introduce post-equalization and several optimization techniques that aims to deal with the problem such as thresholds optimization for PAM-2 and PAM-4, and the two inner levels optimization only for PAM-4.

This Chapter is divided into the following sections :

- **Section 2.1** : we will briefly discuss the equalization concept, highlighting the so called FFE and discussing its principle of operation.
- **Section 2.2** : we will further introduce the optimization techniques that are jointly applied with FFE in mitigate signal-dependant noises.
- **Section 2.3** : we will draw some conclusions

2.1 Equalization

Equalization is a Digital Signal Processing (DSP) technique which is used to reduce distortions affecting transmitted signals. It could be synthesized as a filter with adaptive coefficients. Equalizers, while trained under minimum square error (MSE) criterion, can jointly mitigate inter-symbol interference (ISI) and act as a matched filter. Generally, Adaptive equalizers could be subdivided into two major classes :

- **Linear Equalizer:** It can be implemented in the form of a Finite Impulse Response (FIR) filter: it does not have a feedback. Typical example is the feedforward equalizer (FFE).
- **Non-Linear Equalizer :** particularly used to compensate for severe channel impairments. Typical examples are Decision Feedback Equalizer (DFE) and Volterra non-linear equalizer (VNLE) which based on an expansion of the Taylor series that can generalize a vast variety of time-invariant systems that are dynamic and nonlinear [16].

Since ITU-T had considered a feed-forward equalizer (FFE) option in 50G-PON standard[17], in this Section, we will discuss it.

2.1.1 Feed-forward Equalizer

Feed-forward equalizer can be implemented as a FIR filter with adjustable taps in a transversal structure where the current and the past values of received signals are linearly weighted and summed up to produce the output.

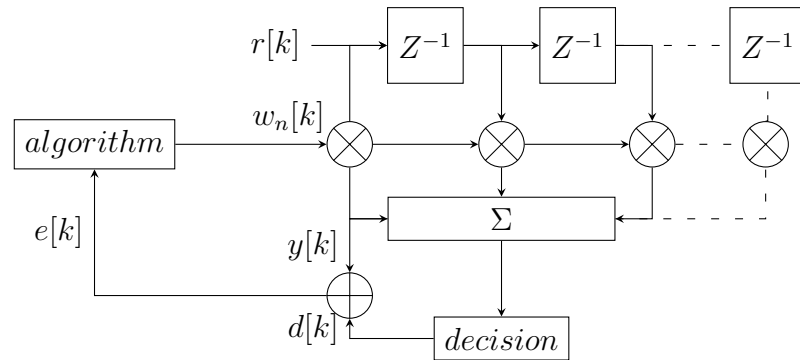


Figure 2.1: Linear equalizer structure: where $r[k]$ is the input sequence, $d[k]$ is the training sequence (also referred to as the desired response), $y[k]$ is the output sequence, $w_n[k]$ are the adjustable equalizer taps

The error signal is used as input to the adaptive algorithm which is in charge of updating weights coefficients.

$$e[k] = d[k] - y[k] \quad (2.1)$$

where $d[k]$ is the training sequence, $r[k]$ is the input sequence, $y[n]$ is the output sequence and $w_n[k]$ is the equalizer taps at discrete time $[k]$.

Generally, the weight adaptation algorithms are gradient based algorithms exploiting Mean Square Error (MSE) as the cost function.

Modified steepest descent method :

The modified steepest descent[18] is an extension of Widrow-Hoff algorithm aiming to minimize $\frac{\partial E\{e^{2n-1}[k]\}}{\partial w[k]}$ for arbitrary choice of $n = 1..2$. The general adaptation rule is :

$$w[k + 1] = w[k] - \frac{1}{2}\mu\nabla \frac{\partial E\{e^{2n-1}[k]\}}{\partial w[k]} \quad (2.2)$$

where n is the order, $w[k + 1]$ is the weight vector at time $k + 1$, $w[k]$ is the weight vector at time k , μ is the step-size parameter also known as learning rate and the last term is the derivative of cost function with respect to the weight taps.

The weight adaptation rule for modified steepest descent is :

$$w[k + 1] = w[k] + \mu E\{e^{2n-1}[k]r[k]\} \quad (2.3)$$

In practice, there are limitations for implementing steepest descent algorithm related to the expectation term $E\{e^{2n-1}[k]r[k]\}$ which is unknown. However, we can estimate it using the sample mean. By considering only one sample to estimate the sample mean we get the so called "LMS".

2.1.2 LMS and LMF Algorithms

LMS is a simplified version of the modified steepest descent method where $n = 1$, expectation is not used and the gradient is approximated [19]. LMS weight adaptation rule is :

$$w[k + 1] = w[k] + \mu e[k]r[k] \quad (2.4)$$

We compared LMS to LMF algorithm performance and we found out that there is no gain in terms of sensitivity. Thus we decided to update the taps of the FFE using LMS algorithm while considering the following parameters :

N-Taps	31
Learning rate μ	10^{-3}

Table 2.1: FFE Parameters

The eye diagrams of PAM-2 and PAM-4 signals after feed-forward equalization are illustrated in Fig.2.2 and Fig. 2.3.

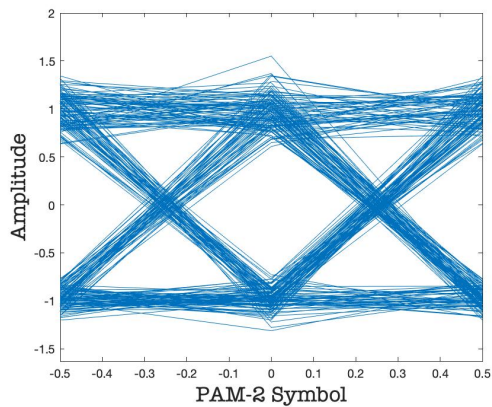


Figure 2.2: Eye-diagram of PAM-2 post-FFE

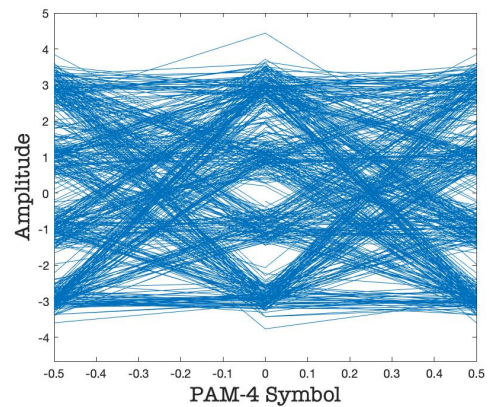


Figure 2.3: Eye-diagram of PAM-4 post-FFE

We can observe that the effect of signal dependent noises (shot and ase) on the signal is still present after equalization because the linear FFE alone was not able to totally eliminate it. Therefore, there will be misjudgments leading to BER deterioration if we relied on the nominal thresholds in decision making.

In the following Chapter we will introduce some optimization techniques to enhance our system performance.

2.2 Techniques of optimization

In this Section, we will introduce two optimization techniques intended to deal with noises of asymmetric nature for each of the modulation schemes in use (PAM-2 and PAM-4), First, we will start with defining the possible degrees of freedom.

For PAM-2 (NRZ), we considered the alphabet $A = [-1, +1]$ and for PAM-4, we considered the alphabet $A = [-3, -1, +1, +3]$. Therefore, the nominal thresholds will be $V_{Th} = [0]$ for NRZ and $V_{Th} = [-2, 0, 2]$ for PAM-4.

The *degrees of freedom for optimization* are shown as solid lines on the eye-diagrams of PAM-2 and PAM-4 in Fig. 2.4 and Fig. 2.5.

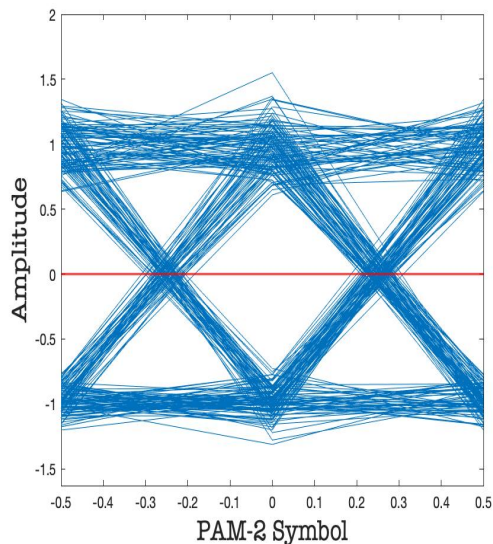


Figure 2.4: Eye-diagram of PAM-2 showing the degree of freedom for optimization

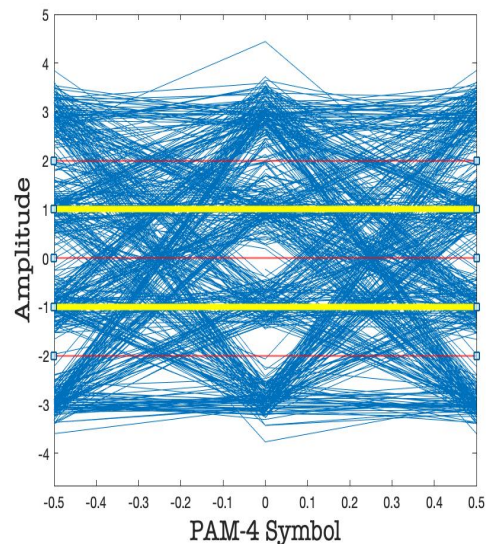


Figure 2.5: Eye-diagram of PAM-4 showing the degrees of freedom for optimization

The only one degree of freedom for optimization in PAM-2 is the decision threshold at the RX. PAM-4 instead benefits from having five different degrees of freedom which are the three decision thresholds at the RX and the two inner levels at the TX.

2.2.1 Thresholds Optimizer

In order to perform thresholds optimization, we followed two different approaches. The first one we studied was based on exhaustive search for thresholds by evaluating system BER at different values of the decision thresholds and then selecting the ones at which BER is minimized.

Exhaustive Search

For an APD receiver, typical example of PAM-2 and PAM-4 BER evaluation at different values of decision thresholds are illustrated in Fig. 2.6 and in Fig. 2.7.

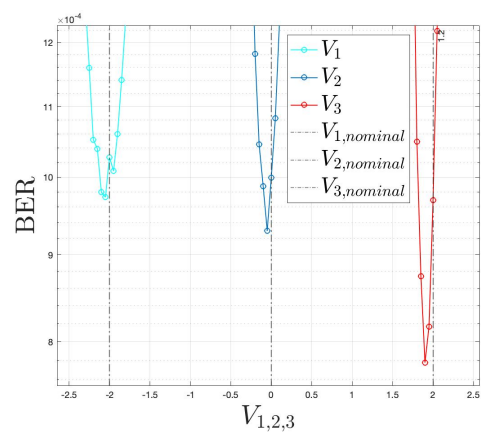
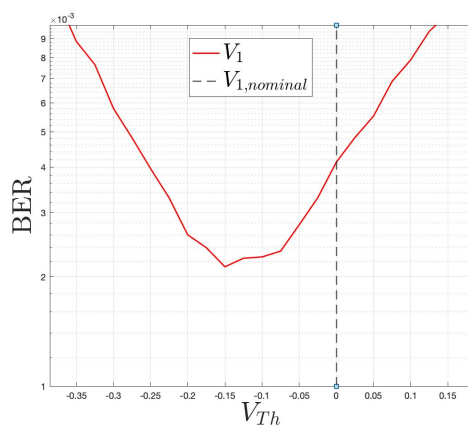


Figure 2.6: PAM-2 V_{Th} vs BER curve at ER of 9 dB and OPL of 27 dB **Figure 2.7:** PAM-4 $V_{1,2,3}$ vs BER curve at ER of 6 dB and OPL of 17 dB

By considering the dashed lines to be the nominal PAM-2 and PAM-4 thresholds, we can notice in both cases that the minimum BER was not found to be at the nominal threshold because of the unbalanced noise variance: the most significant improvement for PAM-4 is achieved by optimizing V_3 which lies between the two upper most levels.

In the second approach instead, we built an optimizer relying on a closed-form calculation with a small approximation: the probability density functions (p.d.f.) of the equalized RX symbols, conditioned on the TX PAM- M level, are assumed to correspond to M independent different Gaussian distributions.

Threshold Optimizer Principle of operation :

An illustration of threshold optimizer building-blocks is in Fig. 2.8

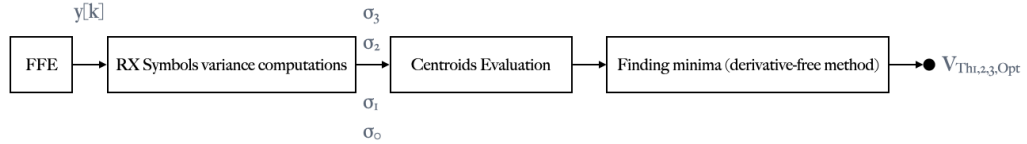


Figure 2.8: Threshold Optimizer building-blocks

Considering the digitized equalized samples (post-FFE) to be the entry data to the optimizer, the following operations are carried out: first, the variance of each of the received symbols are computed. After that, the centroids are evaluated. Finally, thresholds are found by means of a derivative-free method: where the derivative (gradient) is not used and are returned to be used for decision making.

By applying the previously mentioned threshold optimizer in the same working conditions, the PDFs, RX symbols centroids and the optimum thresholds as shown in Fig. 2.9 and Fig. 2.10.

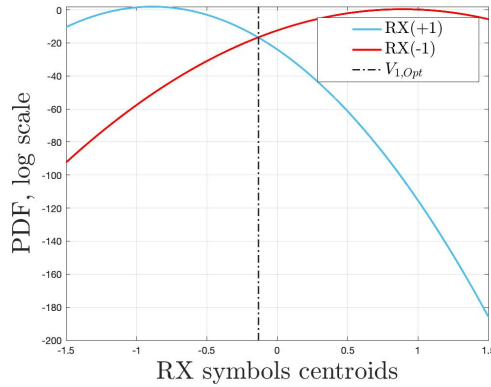


Figure 2.9: $V_{1,Opt}$ for NRZ at ER of 9 dB, $f_{3,dB}$ of 35 GHz and OPL of 27 dB

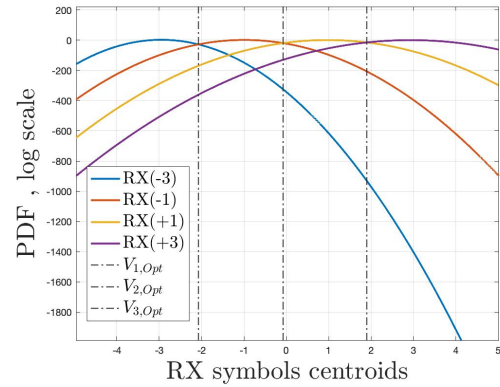


Figure 2.10: $V_{1,2,3,Opt}$ for PAM-4 at ER of 6 dB, $f_{3,dB}$ of 35 GHz and OPL of 17 dB

We can notice that the results we get applying the two approaches coincide with each other but the second approach is significantly faster.

2.2.2 Levels Optimizer

We considered for PAM-4 inner levels optimization a simple grid-search approach: we evaluated the BER over a manually specified subset of the inner levels search space, looking for the combination giving the best performance.

APD-RX

In Fig. 2.11, we show BER evaluation as we optimize the inner levels for APD receiver (i.e., with OPL=17 dB, ER=6 dB).

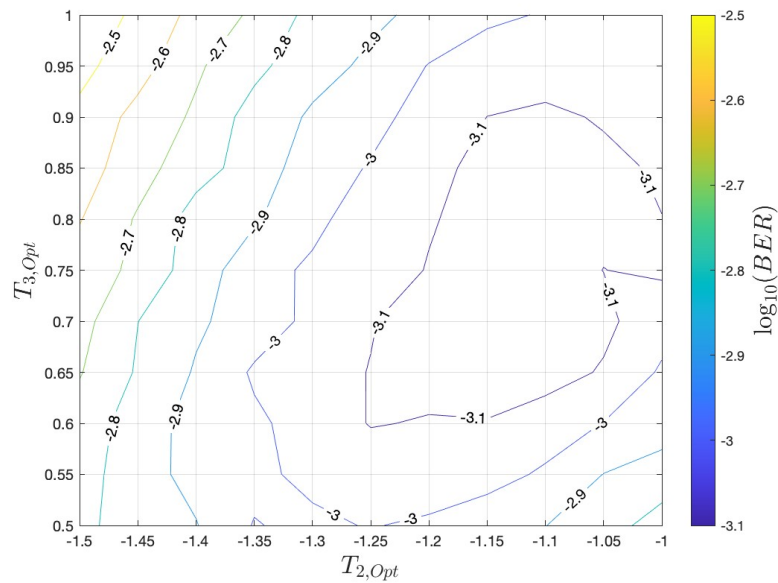


Figure 2.11: Contour plot of PAM4 inner levels for APD at ER of 6 dB, $f_{3dB,electrical}$ of 35 GHz and OPL of 17 dB

We can notice that the optimum levels lie inside the most inner circle (below the nominal levels) with a remarkable gain in terms of BER for this particular case. One possible combination for optimum PAM-4 inner levels for an APD receiver is reported in Tab. 2.2

$T_{2,Opt}$	-1.25
$T_{3,Opt}$	0.65

Table 2.2: PAM-4 optimum inner levels for APD receiver

SOA+PIN-RX

Correspondingly, the same approach had been used to find the optimum inner levels for SOA+PIN.

An example of a grid-search based TX levels optimization for SOA+PIN (i.e., with OPL=21 dB, ER=9 dB) is illustrated in Fig. 2.12.

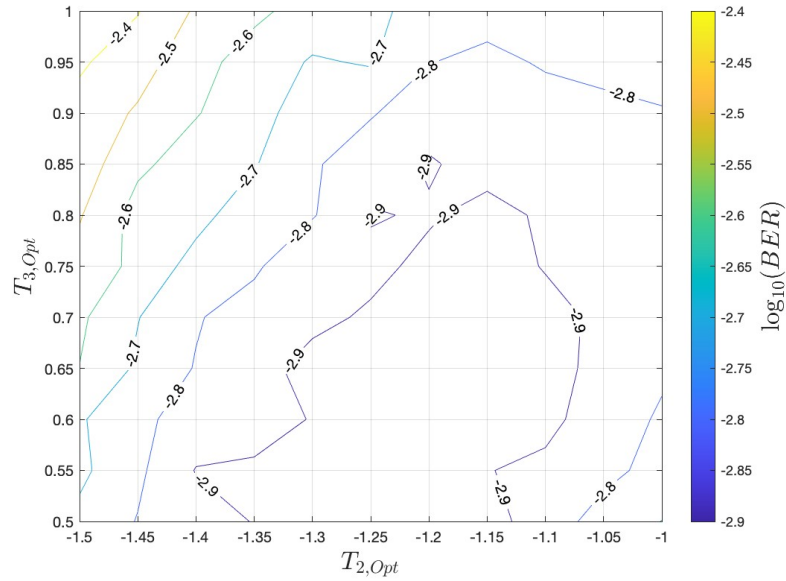


Figure 2.12: Contour plot of PAM4 inner levels for SOA+PIN at ER of 9 dB, $f_{3dB,electrical}$ of 35 GHz and OPL of 21 dB

We notice that BER is enhanced as the inner levels go below the nominal ones just like APD. A possible PAM-4 inner levels composition for a SOA+PIN receiver is reported in Tab. 2.3

$T_{2,Opt}$	-1.25
$T_{3,Opt}$	0.65

Table 2.3: PAM-4 optimum inner levels for SOA+PIN receiver

2.3 Conclusions

In this Chapter we introduced the concept of feed-forward equalization in PON. we investigated both PAM-2 and PAM-4 at 50 Gbps and 100 Gbps without introducing any bandwidth limitations. We found out that the noise asymmetry is still present on the equalized symbols. So we considered optimizing the thresholds and the inner levels.

For what concerns thresholds optimization, we applied two approaches. the first is based on an exhaustive search while the other is based on the assumption of Gaussian PDF of RX symbols.

PAM-2

An example of PAM-2 eye-diagram with signal dependent noise after threshold optimization is provided in Fig.2.13

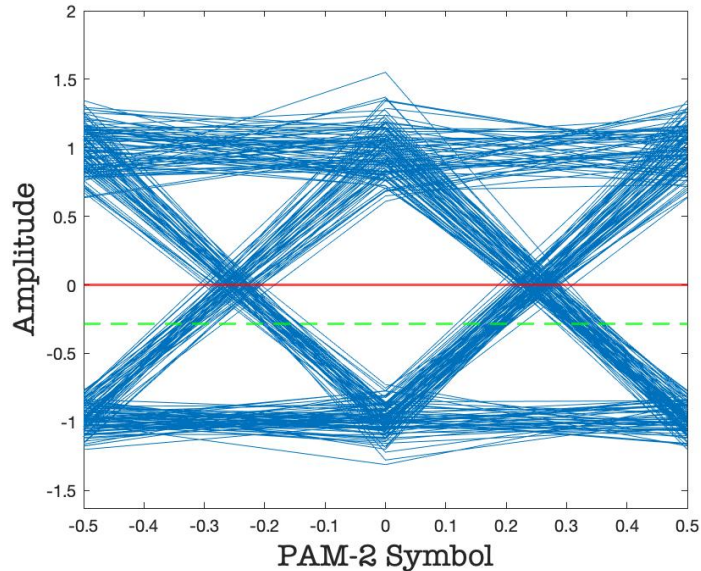


Figure 2.13: Eye-diagram of PAM-2 with threshold optimization at ER of 9 dB and OPL of 21 dB

In case of SOA or APD noise where the higher levels get more affected than the lower ones, PAM-2 threshold was found to be below the nominal one.

For PAM-4, we considered two strategies, the first one was optimizing the three thresholds only while the second strategy was jointly optimizing levels and thresholds.

PAM-4

Typical examples for optimizing only the decision thresholds is illustrated in Fig.2.14. another example for thresholds and levels optimization is shown in Fig. 2.15.

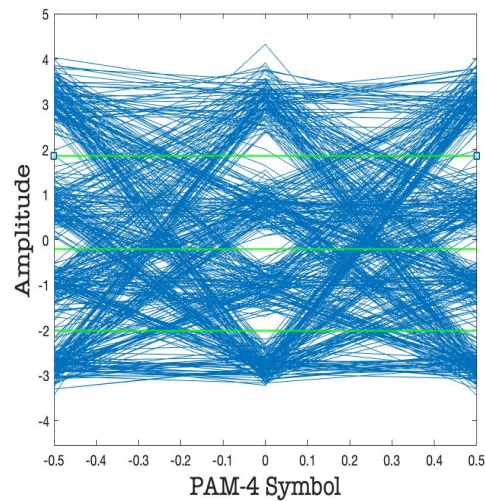
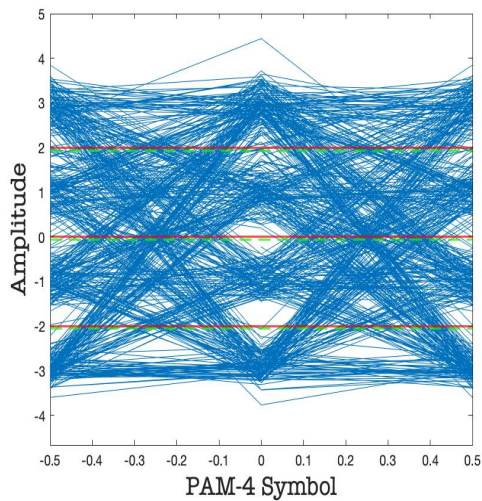


Figure 2.14: Eye-diagram of PAM-4 with threshold optimization at ER of 6 dB and OPL of 17 dB

Figure 2.15: Eye-diagram of PAM-4 with threshold and levels optimization at ER of 6 dB and OPL of 17 dB

We observe by optimizing thresholds only that the optimum thresholds were also found to be slightly below the nominal ones (dash-marked in green) and by referring to Fig. 2.7 the possible BER enhancement is negligible. Whereas, by optimizing thresholds and levels jointly, the eye-diagram becomes more open.

In the next Chapter, we will perform simulations of an APD-RX to demonstrate if the optimization would lead to any significant improvement.

Chapter 3

APD Simulations

In a PON APD-based receiver, as the analog signal passes through a communication link and arrives at the receiver front-end, it gets affected by APD shot noise and TIA thermal noise which effects remain present even after the signal has been equalized and digitized.

In this Chapter, we will investigate the effect of APD shot noise on the system performance in a back-to-back scenario by means of computer simulations while exploiting a trained feed-forward equalizer and the optimization techniques intended for PAM-2 and PAM-4 modulations. The programming environment is purely Matlab.

This Chapter is divided into the following Sections :

- **Section 3.1** : the simulation setup for an APD based-receiver is illustrated.
- **Section 3.2** : we will assess the effectiveness of threshold optimization for a system relying on PAM-2 in terms of optical path loss at different values of extinction ratios and 3-dB bandwidth of the transmitter.
- **Section 3.3** : we will further assess the effectiveness of threshold and levels optimization for a system relying on PAM-4 in terms of optical path loss at different values of extinction ratios and 3-dB bandwidth of the transmitter.
- **Section 3.4** : We draw some conclusions on the results we obtained in this chapter.

3.1 Simulation setup of the APD-based receiver

In this Section, we setup the simulation by grouping up a transmitter that generates the desired symbols, an optical link that introduces attenuation and an APD receiver, where the system impairments show up, and in particular, shot and thermal noises. In Fig. 3.1, the simulated optical system is illustrated.

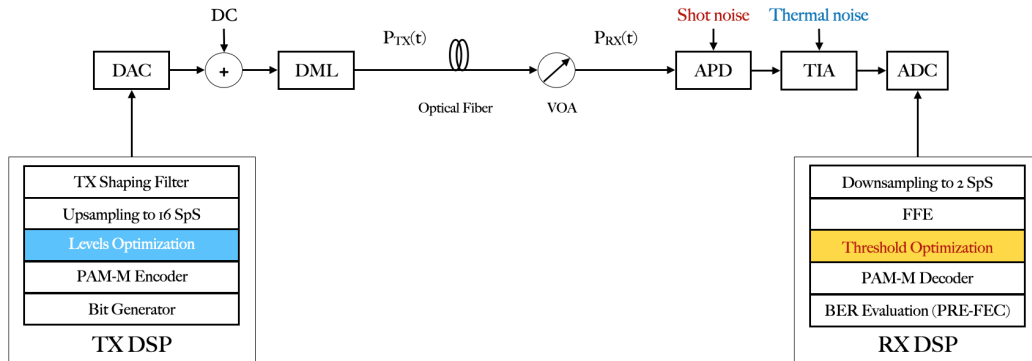


Figure 3.1: APD Simulation Setup

In order to reduce the effect of the APD shot noise, we implemented a threshold optimizer at the receiver side which is generic for NRZ and PAM-4: it operates on the equalized symbols (Post-FFE) and an inner levels optimizer strictly dedicated to PAM-4 at the transmitter side.

We considered the optical path loss to be the primary assessment criterion for the APD receiver.

For simplicity, the following assumptions has been made :

- Ideal DAC / ADC
- Ideal directly modulated laser (DML)
- No chromatic dispersion
- No fiber non-linearities or attenuation
- no bandwidth limitations at the receiver

Transmitter (OLT) :

In a 50G-OE system, a Pseudo Random Binary Sequence (PRBS) is coded to generate PAM-M symbols ($M=2, 4$), followed by a DAC performing conversion and upsampling to 16 *SpS*. The samples are shaped by means of an *electrical Bessel fourth-order filter* having $f_{3dB} = 35 \text{ GHz}$ (i.e corresponding to 70% of the Baud rate). The signal drives an ideal intensity modulator (IM) giving rise to instantaneous power $P_{Tx}(t)$ to be sent over the channel.

Link (ODN) :

We will not consider the effects due to propagation in fiber the linear: chromatic dispersion and attenuation and the non-linear effects. The link can hence be regarded as a Back-to-Back, where the only considerable effect is the attenuation due to a variable optical attenuator (VOA) which applies an attenuation L_{OPL} on the transmitted power where OPL stands for *Optical Path Loss*.

$$P_{Rx}(t) = \frac{P_{Tx}(t)}{L_{OPL}} \quad (3.1)$$

APD Receiver (ONU) :

Upon optical field reception, an Avalanche photo-diode is used to convert signal from optical to electrical domain followed by a low noise TIA converting photocurrent into voltage. Then the signal is digitized (downsampled to 2 *SpS*) and processed using a 31-taps FFE. The equalizer is trained using a sequence identical to the of the original transmitted symbols (before upsampling). The equalizer is then switched to tracking, samples are decoded and BER is evaluated.

Simulation parameters [20] are reported in Tab. 3.1

Simulation Parameters		
APD Responsivity R	0.7	A/W
APD Gain M	10	dB
APD Excess noise figure F_{dB}	7.1	dB
TIA Input-Referred Noise Density $IRND$	15	pA/\sqrt{Hz}
Sampling frequency f_s	800	$GSample/sec$

Table 3.1: Simulation parameters for the APD receiver

3.2 PAM-2 Performance analysis

Using NRZ, the effect of shot noise on the system performance at BER_t of 10^{-2} and 10^{-3} can be shown by evaluating BER vs. ROP.

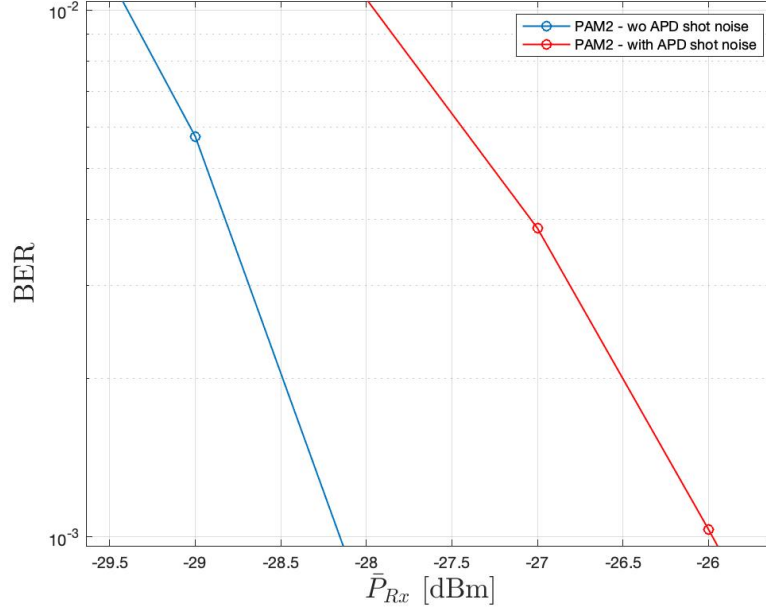


Figure 3.2: ROP vs. BER curve for NRZ at ER of 9 dB and $f_{3dB,electrical}$ of 35 GHz

We can observe in Fig. 3.2 that the shot noise variance dominates the thermal noise variance, putting our system in a shot noise-limited regime and leading to an increasing penalty in terms of ROP as we target higher BER . Typical examples of the penalties in terms of ROP due to shot noise at BER_t of 10^{-2} and at BER_t of 10^{-3} are reported in Tab. 3.2 :

$BER_t = 10^{-2}$	1.5 dB
$BER_t = 10^{-3}$	2.2 dB

Table 3.2: APD shot noise penalty

Now in order to have a better understanding of the problem, in the following Sections we will evaluate the system performance at different values of extinction ratios and bandwidth limitations.

3.2.1 Assessment against various extinction ratios

Considering a constant average transmitted power \bar{P}_{Tx} of 0 dBm, the extinction ratio will be a possible degree of freedom since it defines the separation between the two PAM-2 levels. The higher the extinction ratio, the wider the separation. Thus, the less severe the impact of APD shot noise on BER will be.

In Fig. 3.3 we show the results of evaluating Optical Path Loss versus Extinction ratio at BER_t of 10^{-2} with and without *shot noise* while having no bandwidth limitations ($f_{3dB,electrical}$ at 35 GHz).

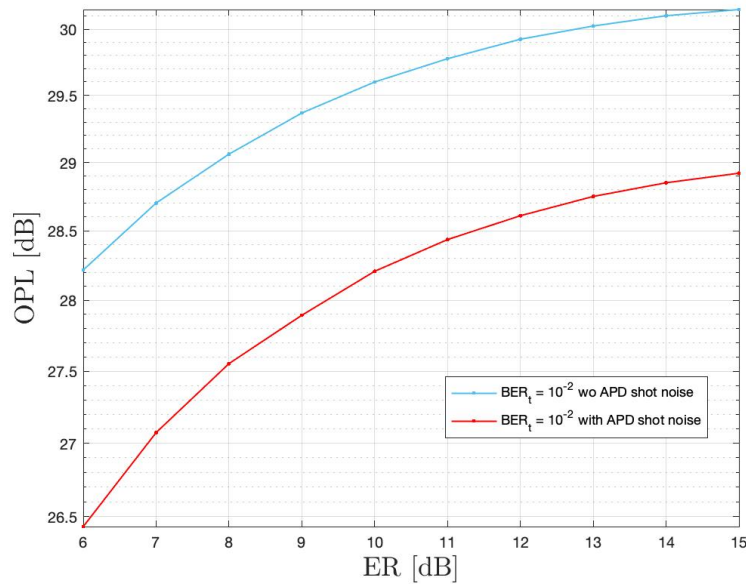


Figure 3.3: ER vs. OPL curves with and without shot noise for NRZ

First, we observe a gain of about 2.5 dB for operating at 15 dB of ER compared to 6 dB in a shot noise-limited regime. Second, we notice higher penalties due to shot noise at lower values of extinction ratio that is due to the fact that the levels which are affected by unbalanced noise distributions get closer to each others.

Threshold optimization

As shot noise is considered a signal-dependent noise variance of an asymmetric nature, we will consider the compensation procedure of dynamically adjusting the threshold in receiver DSP.

In Fig. 3.4 we demonstrate the results of evaluating Optical Path Loss versus Extinction ratio at BER_t of 10^{-2} and BER_t of 10^{-3} with and without threshold optimization in a shot noise limited regime.

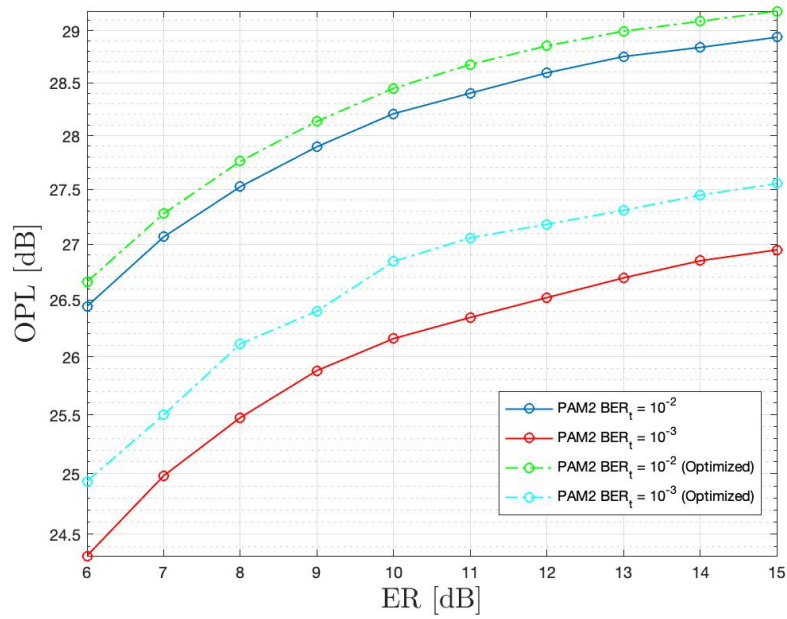


Figure 3.4: ER vs. OPL curve with and without threshold optimization relevant to NRZ at $f_{3dB,electrical}$ of 35 GHz

We notice that APD-based receivers benefit from optimizing the decision thresholds when transmitting NRZ signals, with an almost constant gain of OPL for every considered ER. The sensitivity enhancements at ER of 9 dB of ER are reported in Tab. 3.3:

$BER_t = 10^{-2}$	0.2 dB
$BER_t = 10^{-3}$	0.6 dB

Table 3.3: APD sensitivity enhancement at 9 dB of ER

3.2.2 Assessment against 3-dB bandwidth of transmitter

Operating at a high bit rate comes at the cost of distorting the signal due to the bandwidth limitations of the filters in use. In particular, APD receivers could suffer from a huge bandwidth limitation due to the intrinsic gain which implies, by default, huge capacitance. In this section we will consider bandwidth limitations due to transmitter shaping filter.

In Fig. 3.5 we show the results of evaluating Optical Path Loss versus 3-dB bandwidth of the transmitter filter normalized by the baud-rate at BER_t of 10^{-2} with and without *shot noise* at ER of 9 dB while having a FFE implemented.

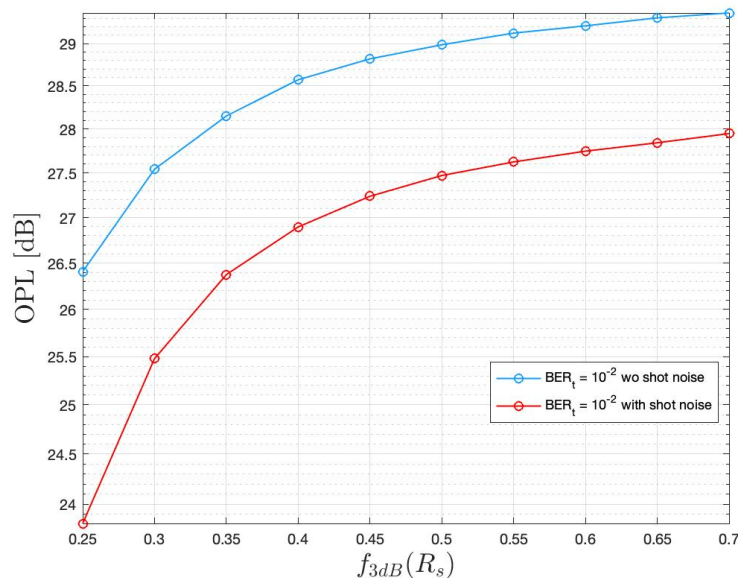


Figure 3.5: $f_{3dB,electrical}$ vs. OPL curve with and without shot noise for NRZ at BER_t of 10^{-2}

In a bandwidth-limited regime ($f_{3dB} < 0.5R_s$), we observe a fast performance degradation in both scenarios: with and without shot noise. In addition, we observe that the effect of shot noise becomes more significant at lower f_{3dB} . The penalty due to shot noise at f_{3dB} of $0.3R_s$ is reported in Tab. 3.4

$BER_t = 10^{-2}$	2.1 dB
-------------------	--------

Table 3.4: APD shot noise penalty at f_{3db} of $0.3 R_s$ for PAM-2

Threshold optimization

In Fig. 3.6 we show the results of evaluating Optical Path Loss versus 3-dB bandwidth normalized by the baud-rate at BER_t of 10^{-2} and at BER_t of 10^{-3} with and without threshold optimization in a shot noise limited regime.

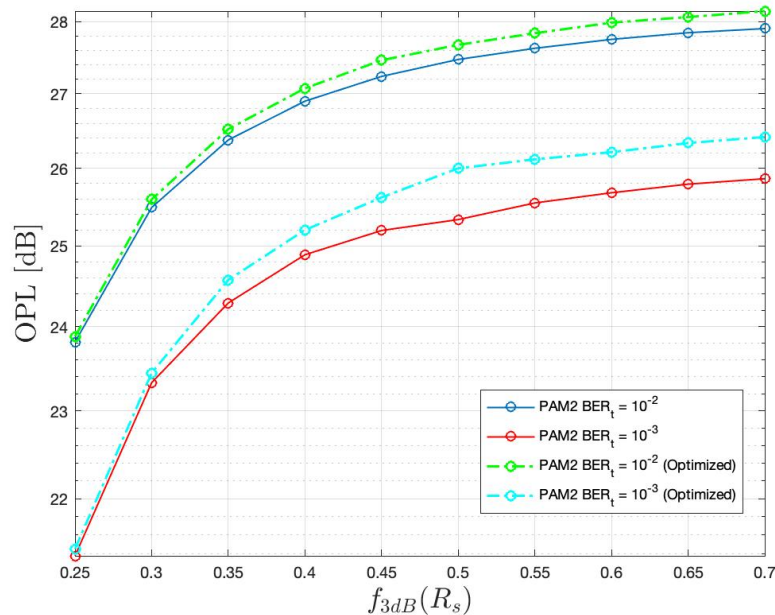


Figure 3.6: $f_{3dB,electrical}$ vs. OPL curve with and without threshold optimization relevant to NRZ at ER of 9 dB

An important remark on the results shown in this figure is that threshold optimization is totally insignificant at $f_{3dB} < 35\%$ of the baud rate while, in fact, shot noise is higher. This is likely due to the fact that the APD noise asymmetry is averaged out by the FFE that, in order to compensate for inter-symbol interference, it correlates several consecutive symbols with a given impulse response.

The sensitivity enhancements for ($f_{3db} > 0.5 R_s$) are reported in Tab. 3.5:

$BER_t = 10^{-2}$	0.15 dB
$BER_t = 10^{-3}$	0.5 dB

Table 3.5: APD sensitivity enhancement

3.3 PAM-4 Performance analysis

PAM-4 is currently being considered for 100G passive optical networks allowing transmission of twice the bit rate (R_b) of a NRZ over approximately the same baud-rate. However, the use of a multi-level format implies reduced receiver sensitivity as the signal becomes more vulnerable to distortion.

The effect of shot noise on a PAM-4 system performance at BER_t of 10^{-2} and 10^{-3} can be illustrated by evaluating BER versus ROP.

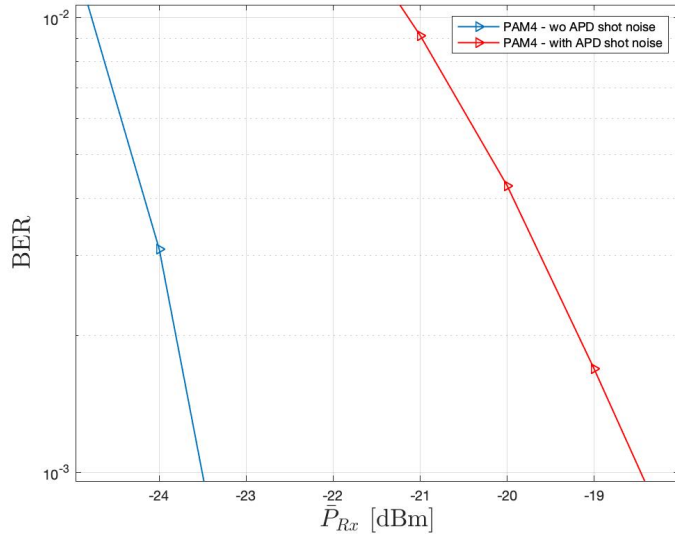


Figure 3.7: ROP vs. BER curve for PAM4 at ER of 9 dB and $f_{3dB,electrical}$ of 35 GHz

We can notice that a system using PAM-4 is also limited by shot noise and the penalty is higher for PAM-4 than for a NRZ. The reason behind higher penalty in PAM-4 is that shot noise affects four levels instead of two in PAM-2. In addition, this penalty increases at higher BER_t . Typical examples of the penalties at 10^{-2} and at $BER_t = 10^{-3}$ are reported in Tab.3.6

	PAM-4	PAM-2
$BER_t = 10^{-2}$	3.6 dB	1.5 dB
$BER_t = 10^{-3}$	5 dB	2.2 dB

Table 3.6: APD shot noise penalty for PAM4 vs. PAM-2

3.3.1 Assessment against various extinction ratios

For PAM-4, the extinction ratio defines the separation between the two outer levels. The higher the extinction ratio, the wider the separation.

In Fig. 3.8 we show the results of evaluating Optical Path Loss versus Extinction ratio for PAM-4 at BER_t of 10^{-2} with and without *shot noise* while having no bandwidth limitations ($f_{3dB,electrical}$ at 35 GHz).

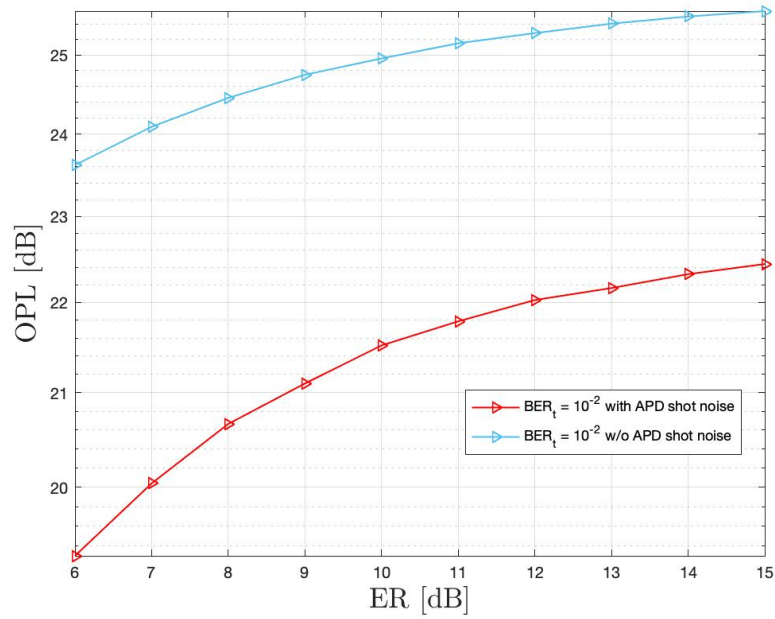


Figure 3.8: ER vs. OPL curves with and without shot noise for PAM-4

Similarly to NRZ case, we observe that the penalty due to shot noise is higher at lower values of extinction ratios because the asymmetric nature of the noise is preserved when the system is not affected by huge bandwidth limitations and the power levels get closer to each others.

Threshold optimization

By considering only thresholds optimization for PAM-4, we illustrate the results of evaluating Optical Path Loss versus Extinction ratio at BER_t of 10^{-2} and BER_t of 10^{-3} in Fig. 3.9.

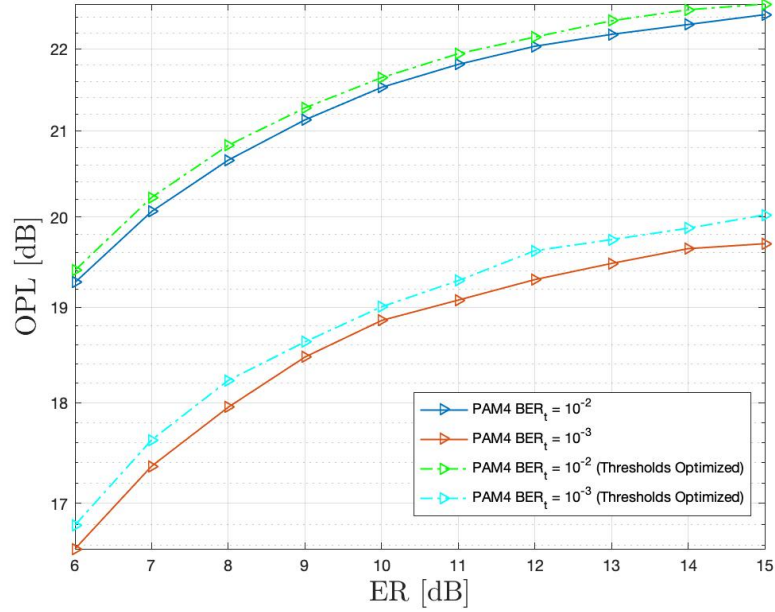


Figure 3.9: ER vs. OPL curve with and without thresholds optimization relevant to PAM-4 at $f_{3dB,electrical}$ of 35 GHz

We can see that the improvements we have in terms of OPL are negligible (around 0.2 dB) at BER_t of 10^{-2} and BER_t of 10^{-3} even less than NRZ, that is due to the fact that, in PAM-4: at the nominal levels, the optimum threshold is constrained in a tight region between these levels. We can also notice that thresholds optimization gain is almost persistent for all values of ER in range. The sensitivity enhancements for PAM-4 are reported in Tab. 3.7:

$BER_t = 10^{-2}$	0.2 dB
$BER_t = 10^{-3}$	0.3 dB

Table 3.7: APD sensitivity enhancement for PAM-4 after optimizing thresholds for PAM-4

Thresholds and levels optimization

We also tried to jointly optimize thresholds and levels (outer OMA): using the grid-search-based approach we picked up the values of inner levels reported in Tab. 2.2.

We illustrate the results of evaluating Optical Path Loss versus Extinction ratio at BER_t of 10^{-2} and BER_t of 10^{-3} :with and without optimization.

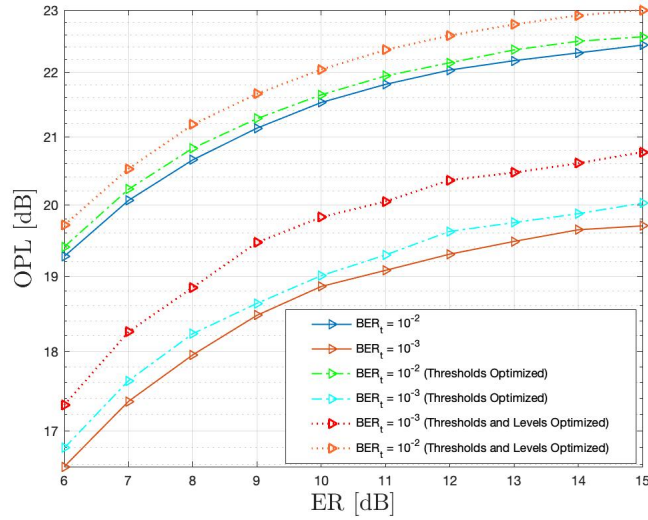


Figure 3.10: ER vs. OPL curve with and without thresholds and levels optimization relevant to PAM-4 at $f_{3dB,electrical}$ of 35 GHz

We can notice with the joint optimization that there is a remarkable improvement in terms of OPL (around 1 dB of OPL) for all values of extinction ratios. The reason behind this is that the optimized levels reduces the probability of error: making the eye-diagram more. The maximum achievable OPL gains are reported in Tab. 3.8 :

$BER_t = 10^{-2}$	0.6 dB
$BER_t = 10^{-3}$	1.1 dB

Table 3.8: APD sensitivity improvement after optimizing levels and thresholds of PAM-4

3.3.2 Assessment against 3-dB bandwidth of transmitter

In Fig. 3.11 we show the results of evaluating Optical Path Loss versus 3-dB bandwidth normalized by the baud-rate at BER_t of 10^{-2} with and without *shot noise* (at ER of 9 dB).

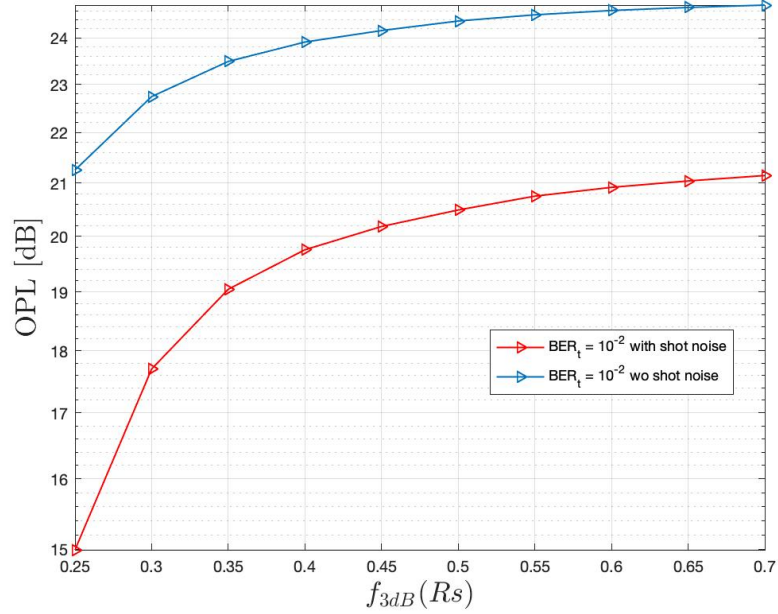


Figure 3.11: $f_{3dB,electrical}$ vs. OPL curve with and without shot noise for PAM-4

Analyzing our PAM-4 system while introducing transmitter bandwidth limitations shows similar results to our previous observations. the penalty is higher at lower values of f_{3dB} .

In Tab. 3.9 we report the penalty due to shot noise at $f_{3dB} = 0.3R_s$:

$$\overline{BER_t = 10^{-2} \quad 5.0 \text{ dB}}$$

Table 3.9: APD shot noise penalty at f_{3db} of $0.3 R_s$ for PAM-4

Threshold optimization

The effectiveness of threshold optimization for different values of $f_{3dB,electrical}$ was evaluated in a shot-noise limited regime. We plotted the Optical Path Loss versus 3-dB bandwidth normalized by the baud-rate at BER_t of 10^{-2} and at BER_t of 10^{-3} .

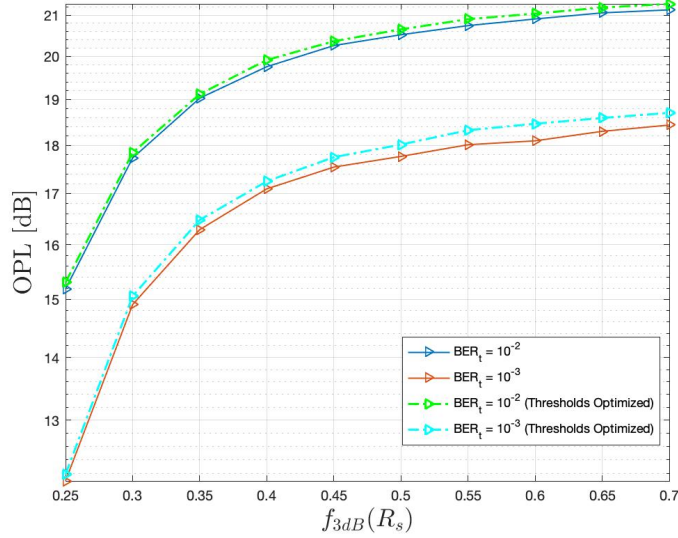


Figure 3.12: $f_{3dB,electrical}$ vs. OPL curve with and without thresholds optimization relevant to PAM-4 at ER of 9 dB

Observably, the improvements we have in terms of sensitivity (OPL) at BER_t of 10^{-2} and BER_t of 10^{-3} after optimizing thresholds only are negligible and they get even worse as we introduce higher bandwidth limitations. The reason behind is that as FFE tries to minimize ISI, it correlates a large number of consecutive symbols with a given impulse response so that the noise variance on the decision variables loses its asymmetric nature. The maximum possible enhancements as we optimize the thresholds only are observed at ($f_{3db} > 0.5 R_s$) and are reported in Tab.3.10:

$BER_t = 10^{-2}$	0.2 dB
$BER_t = 10^{-3}$	0.3 dB

Table 3.10: APD sensitivity enhancement for PAM-4 after optimizing thresholds

Thresholds and levels optimization

In Fig. 3.13 we illustrate the results of evaluating Optical Path Loss versus 3-dB bandwidth normalized by the baud-rate at BER_t of 10^{-2} and BER_t of 10^{-3} with and without the joint optimization of thresholds and levels.

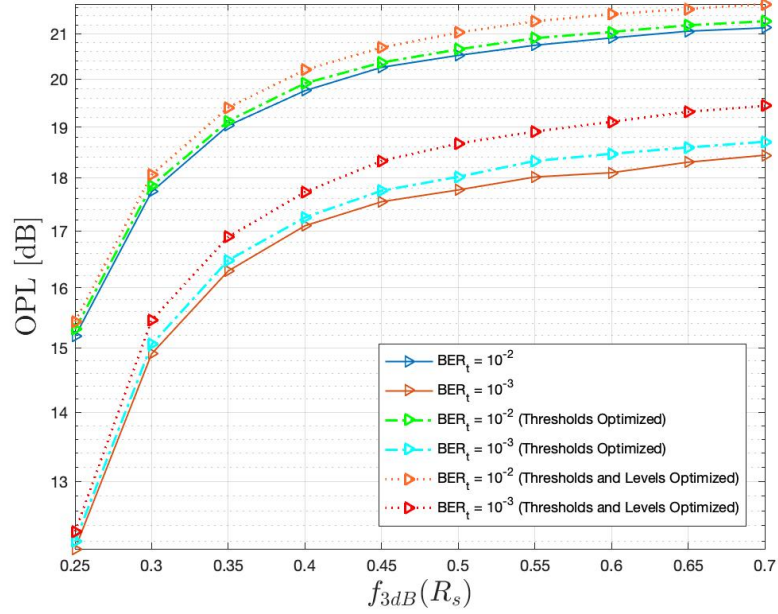


Figure 3.13: $f_{3dB,electrical}$ vs OPL curves with and without threshold and levels optimization relevant to PAM-4 at ER of 9 dB

We notice that optimizing the levels contributes the most in having better sensitivity. but, this effect vanishes gradually at lower 3-dB filter bandwidth because the noise variance tends to be more symmetric.

the sensitivity enhancements at ($f_{3db} > 0.5 R_s$) are reported in Tab. 3.11 :

$BER_t = 10^{-2}$	0.6 dB
$BER_t = 10^{-3}$	1.1 dB

Table 3.11: APD sensitivity enhancement for PAM-4 after optimizing levels and thresholds

3.4 Conclusions

In this chapter, we performed simulations for an APD-based receiver, exploiting a feed forward equalizer and optimization technique, and illustrated the results of applying the optimization techniques on the equalized symbols.

By looking at the results reported in this chapter, several aspects emerge :

- APD shot noise becomes more significant while transmitting a PAM-4 than while transmitting NRZ at the same baudrate.
- Since APD shot noise variance exhibits dependency on the instantaneous received optical power, optimization of thresholds shows a constant gain in terms of OPL for all values of extinction ratios.
- Optimizing PAM-2 threshold in APD-RX shows a considerable gain. Whereas, thresholds optimization for PAM-4 is negligible.
- By introducing huge bandwidth limitations, the analog signal becomes more vulnerable to distortion due to shot noise and as the signal gets digitized and processed by the FFE, the noise asymmetry is averaged out because the FFE considers large number of several consecutive symbols to combat ISI: by correlating them with a given impulse response.
- The optimization of PAM-4 inner levels jointly with thresholds shows a significant sensitivity improvement compared to thresholds only.

In the next Chapter we will consider SOA+PIN receiver as an alternative to the APD receiver, we will analyze its performance while transmitting PAM-2 and PAM-4 in several scenarios: in an optimized and non-optimized schemes.

Chapter 4

SOA+PIN Simulations

In the next generation of passive optical networks (PON), SOA+PIN based receiver may come into practice aiming to provide a higher sensitivity compared to APD-based receiver. However, Semi-conductor optical amplifiers introduce another noise source (ASE noise) on the top of those we considered in the previous chapter.

In this Chapter, we will inspect the effect ASE noise on the system performance in a back-to-back scenario while exploiting an optical filter, a trained feed-forward equalizer and the same optimization techniques of optimizing either thresholds or inner levels.

This Chapter is divided into the following sections :

- **Section 4.1:** the simulation setup for a SOA+PIN based-receiver is illustrated, reporting the simulation parameters and main blocks in use.
- **Section 4.2:** the performance of the optimizer for a system relying on PAM-2 is assessed as a function of optical path loss against different values of extinction ratios, 3-dB bandwidth of transmitter, 3-dB bandwidth of the optical filter and the gain of SOA.
- **Section 4.3:** the performance analysis is extended for PAM-4 and is evaluated in different extinction ratios and bandwidth scenarios.
- **Section 4.4** we conclude the results obtained in this chapter.

4.1 Simulation setup for SOA+PIN receiver

In this Section, we setup the simulation by putting together a transmitter, an optical link and an SOA+PIN receiver where ASE and thermal noises are added. We illustrate the simulated optical system in Fig. 4.1.

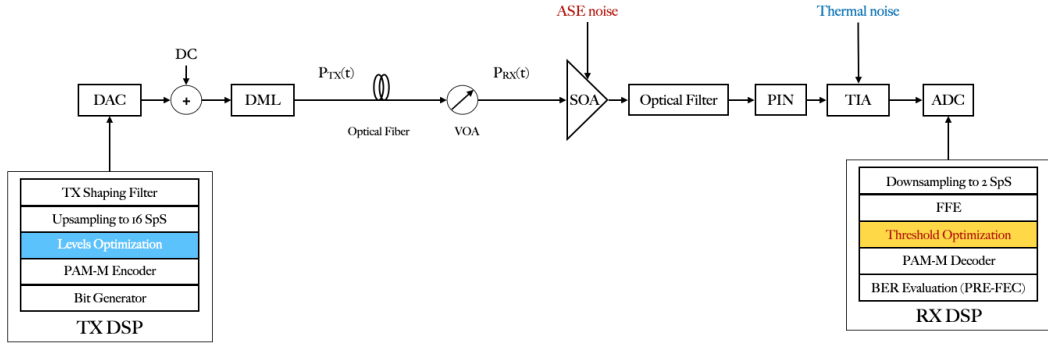


Figure 4.1: SOA+PIN Simulation Setup

In order to mitigate SOA ASE noise, we implemented a threshold optimizer in the receiver DSP that aims to adjust thresholds. Additionally, for PAM-4 inner levels optimization is performed at the transmitter.

Similarly to the APD-RX, the *optical path loss* was considered to be the main assessment criterion for the SOA+PIN receiver.

The following assumptions were made :

- Ideal directly modulated laser (DML)
- Ideal DAC / ADC
- No chromatic dispersion
- No fiber non-linearities
- No SOA non-linearities
- No bandwidth limitations at the receiver

SOA+PIN Receiver :

Upon optical field reception at the front-end, a SOA is used to amplify the signal followed by an optical filter to suppress the noise added by SOA. Then, the signal encounters a PIN and a TIA before it gets down-sampled to 2 SpS using ADC. Lastly, Post-Detection DSP takes place.

Simulation parameters [20] are reported in Tab. 4.1.

Simulation Parameters		
PIN Responsivity R	0.7	A/W
SOA Gain G	15	dB
SOA noise figure F_{dB}	7.5	dB
SOA Pump frequency f_0	228	THz
Optical filter cut-off freq. $f_{3dB,Optical}$	300	GHz
TIA Input-Referred Noise Density $IRND$	15	pA/\sqrt{Hz}
Sampling frequency f_s	800	$GSample/s$

Table 4.1: Simulation parameters for SOA+PIN receiver

4.2 PAM-2 Performances analysis

In Fig. 4.2, the effect of ASE noise on the system performance at BER_t of 10^{-2} and 10^{-3} is shown by evaluating BER vs. ROP.

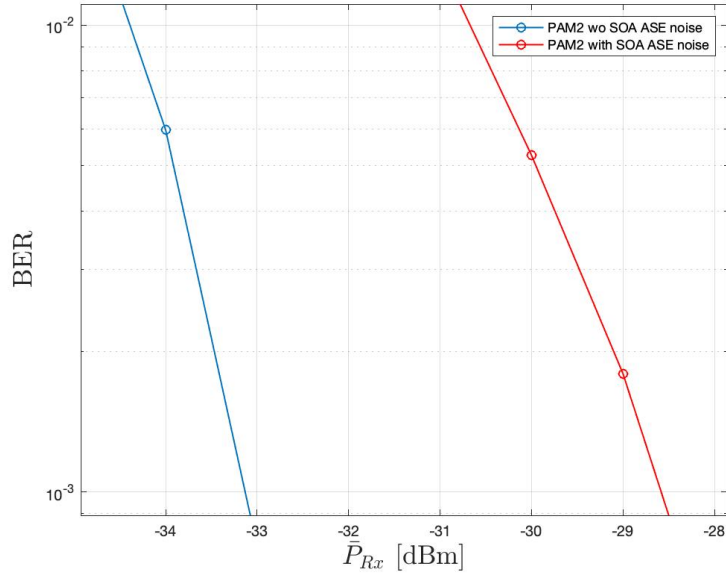


Figure 4.2: ROP vs BER curve for NRZ at ER of 9 dB and $f_{3dB,electrical}$ of 35 GHz

We can notice that the our system is limited by ASE noise with an increasing penalty in terms of ROP at higher BER_t . Typical values of the penalties at BER_t of 10^{-2} and 10^{-3} are reported in Tab. 4.2

$BER_t = 10^{-2}$	3.5 dB
$BER_t = 10^{-3}$	4.5 dB

Table 4.2: SOA ASE noise penalty

Now in order to have a better understanding of the problem, in the following Sections we will evaluate the system performance at different values of extinction ratios and 3-dB bandwidth of the electrical and optical filter.

4.2.1 Assessment against various extinction ratios

Similar to what we had done in PAM-2 APD simulation, Fig. 4.3 shows the results of evaluating Optical Path Loss versus Extinction ratio at BER_t of 10^{-2} with and without *ASE noise* while having no bandwidth limitations ($f_{3dB,electrical}$ at 35 GHz).

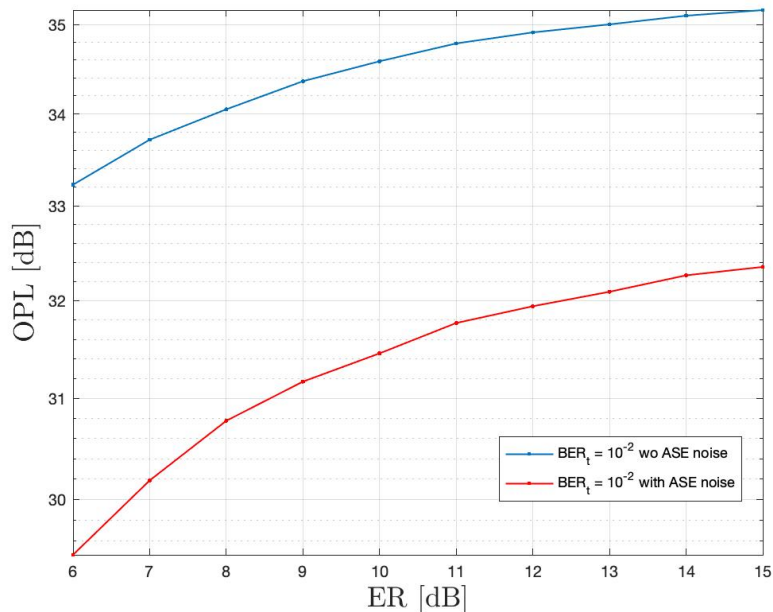


Figure 4.3: ER vs OPL curve with and without ASE noise for NRZ

First, we can notice a gain of 3 dB at ER of 15 dB compared to 6 dB in an ASE noise-limited regime. Second, we can observe higher penalties due to ASE noise at lower values of extinction ratio because the levels that are affected by the unbalanced noise distributions get closer to each others.

Threshold optimization

By considering the procedure of optimizing the threshold at receiver.

In Fig. 3.4 we illustrate the results of evaluating Optical Path Loss versus Extinction ratio at BER_t of 10^{-2} and BER_t of 10^{-3} : with and without threshold optimization in an ASE noise-limited regime.

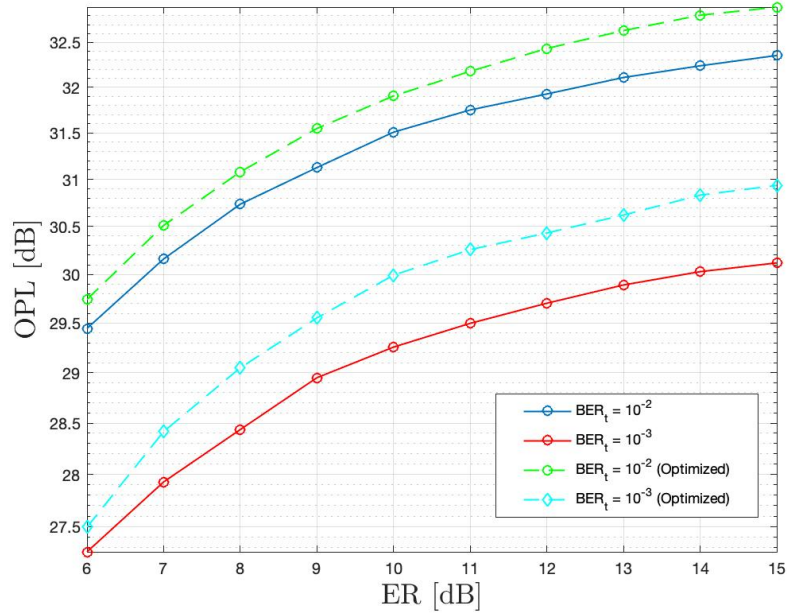


Figure 4.4: ER vs OPL curve with and without threshold optimization relevant to NRZ at $f_{3dB,electrical}$ of 35 GHz

Unlike APD shot noise which exhibits dependency on the instantaneous received optical power, SOA ASE does not. Hence, the ASE noise variance remains constant for all values of extinction ratios in range: what changes is the ratio between ASE and thermal noise. The improvements in terms of OPL at ER of 15 dB are reported in Tab. 4.3:

$BER_t = 10^{-2}$	0.5 dB
$BER_t = 10^{-3}$	0.8 dB

Table 4.3: SOA+PIN sensitivity enhancement at 15 dB of ER

4.2.2 Assessment against 3-dB bandwidth of transmitter

Similarly to APD, we illustrate the results of evaluating Optical Path Loss versus 3-dB bandwidth of transmitter filter normalized by the baud-rate at BER_t of 10^{-2} : with and without *ASE noise* at 9 dB of ER.

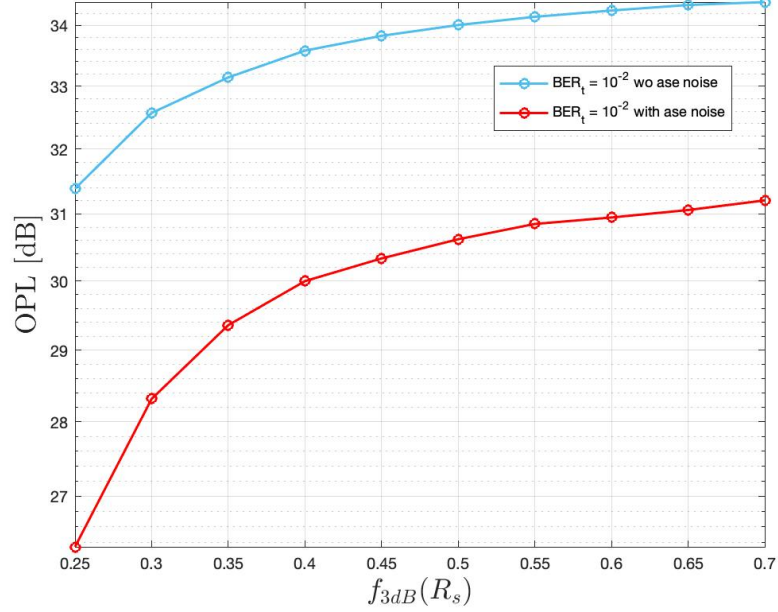


Figure 4.5: $f_{3dB,electrical}$ vs OPL curve with and without ASE noise for NRZ at BER_t of 10^{-2}

In a bandwidth-limited regime ($f_{3dB} < 0.5R_s$), we can observe in Fig. 4.5 a performance degradation in both scenarios: with and without ASE noise. However, the effect of ASE noise is higher for lower values of f_{3dB} (higher bandwidth limitations). In Tab. 4.4 we report the penalty due to ase noise at $f_{3dB} = 0.3R_s$:

$BER_t = 10^{-2}$ 2.2 dB

Table 4.4: SOA ASE noise penalty at f_{3db} of $0.3 R_s$ for PAM-2

Threshold optimization

In Fig. 4.6 we show the results of evaluating Optical Path Loss versus 3-dB bandwidth normalized by the baud-rate at BER_t of 10^{-2} and at BER_t of 10^{-3} : with and without threshold optimization in an ASE noise limited regime.

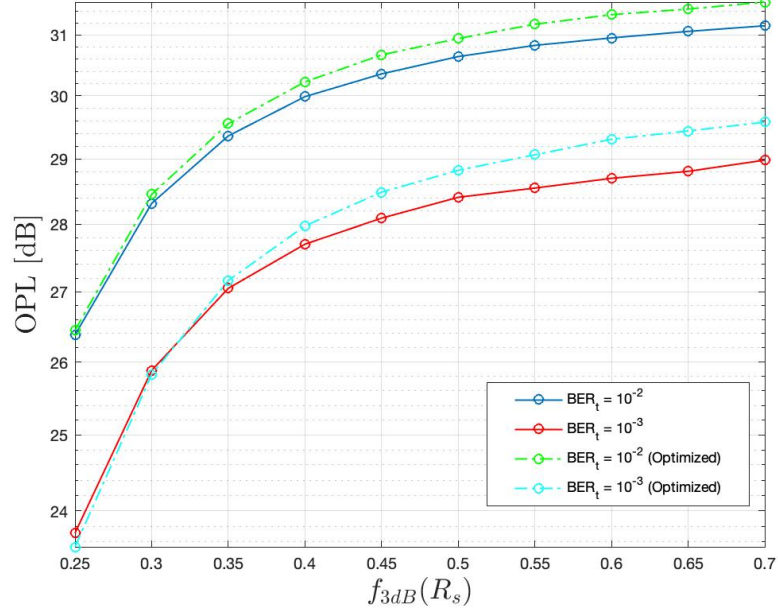


Figure 4.6: $f_{3dB,electrical}$ vs OPL curve with and without threshold optimization relevant to NRZ at ER of 9 dB

We noticed that threshold optimization gain was totally negligible at $f_{3,dB} < 35$ percent of the baud rate, This is likely because the FFE average the noise out by correlating large number of consecutive symbols with a given impulse response. Another important remark is that by allocating more bandwidth, the effectiveness of threshold optimization increases that is due to the fact that the ratio between thermal to ASE noise changes in the same fashion. The maximum enhancements in terms of OPL are reported in Tab. 4.5 :

$BER_t = 10^{-2}$	0.15 dB
$BER_t = 10^{-3}$	0.5 dB

Table 4.5: SOA+PIN sensitivity enhancement at $f_{3dB,electrical}$ of $0.7 R_s$

4.2.3 Assessment against optical amplifier gain

SOA gain is an important parameter, the higher gain, the better sensitivity. However, we must know to what extent raising the gain might be useful.

In Fig. 4.7 we show the results of evaluating Optical Path Loss versus SOA gain at BER_t of 10^{-3} : with and without optimization.

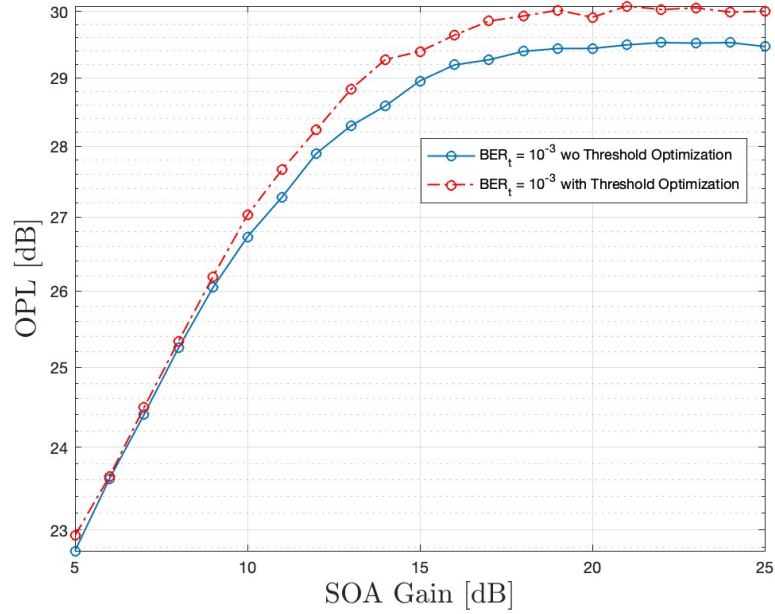


Figure 4.7: SOA gain vs OPL curve with and without threshold optimization for NRZ

We observe an asymptotic behavior up to a gain of 10 dB where threshold optimization was found to be useless then the curve starts being non linear before it goes into a region of saturation. This behaviour is likely, due to the fact that, ASE noise variance exhibits dependency on the amplifier gain. Thus, at lower gain, the thermal noise dominates the ASE noise while at higher gains, ASE noise dominates thermal noise. The sensitivity improvements in terms of OPL in the saturation region at BER of 10^{-3} is reported in Tab. 4.6 :

$$\overline{BER_t = 10^{-3} \quad 0.4 \text{ dB}}$$

Table 4.6: SOA+PIN sensitivity enhancement at BER_t of 10^{-3}

4.2.4 Assessment against 3-dB bandwidth of optical filter

We will consider now bandwidth limitations due to the optical filter in use.

In Fig. 4.8 we show the results of evaluating Optical Path Loss versus 3-dB bandwidth of optical filter at BER_t of 10^{-3} with and without optimization.

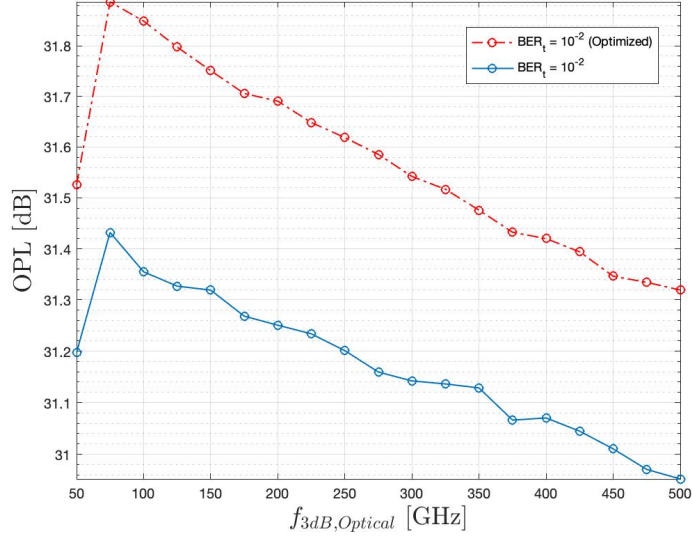


Figure 4.8: $f_{3dB,optical}$ vs OPL with and without threshold optimization relative to NRZ

We can notice for the values of cut-off frequency below 70 GHz that the system performance is degraded in terms of OPL. This performance degradation is likely because, the filter cuts off a portion of the useful signal. Afterwards, as the 3-dB bandwidth of the optical filter gets larger, more ASE noise passes through the filter leads to penalty in terms of OPL. Moreover, we can achieve a constant gain in terms of OPL for all values of filter cut-off frequencies by optimizing the threshold. In Tab. 4.7 we report the gain of optimizing the threshold.

$$\underline{\underline{BER_t = 10^{-2} \quad 0.4 \text{ dB}}}$$

Table 4.7: SOA+PIN sensitivity enhancement at $f_{3dB,optical}$ of 300 GHz for NRZ

4.3 PAM-4 Performance analysis

Similar to what had done for APD simulations in Sec. 3.3, we analyze the effect of ASE noise on the system performance at BER_t of 10^{-2} and 10^{-3} by evaluating BER over ROP.

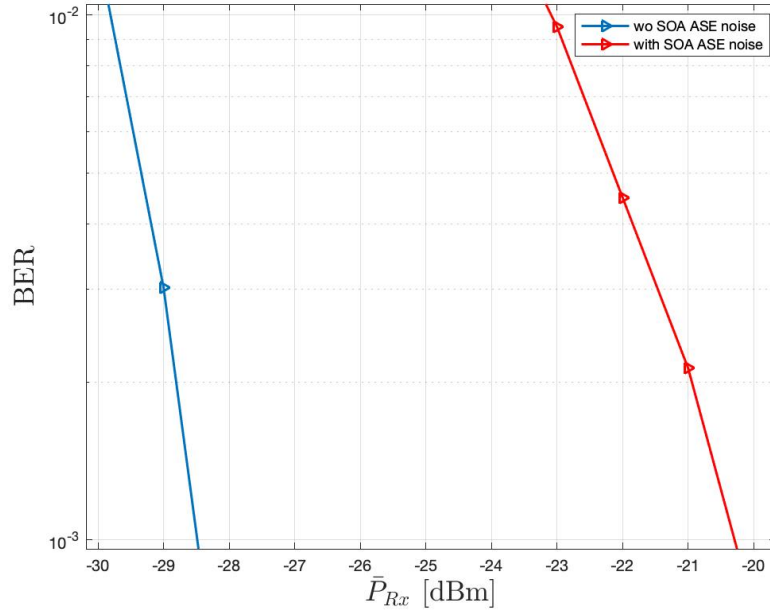


Figure 4.9: ROP vs BER for PAM4 at ER of 9 dB and $f_{3dB,electrical}$ of 35 GHz

We can notice that a system using PAM-4 is also limited by the ASE noise and has a greater penalty in terms of OPL than in NRZ: the ASE noise affects more power levels. Moreover, this penalty increases at a higher BER_t . Typical examples of the penalties at 10^{-2} and at $BER_t = 10^{-3}$ are reported in Tab.4.8

	PAM-4	PAM-2
$BER_t = 10^{-2}$	6.7 dB	3.5 dB
$BER_t = 10^{-3}$	8.3 dB	4.5 dB

Table 4.8: SOA ASE noise penalty for PAM4 vs. PAM-2

4.3.1 Assessment against various extinction ratios

Similar to what we had done for APD simulations in Sec. 3.3.1, The results of evaluating Optical Path Loss versus Extinction ratio for PAM-4 at BER_t of 10^{-2} : with and without *ASE noise* are illustrated in Fig. 4.10.

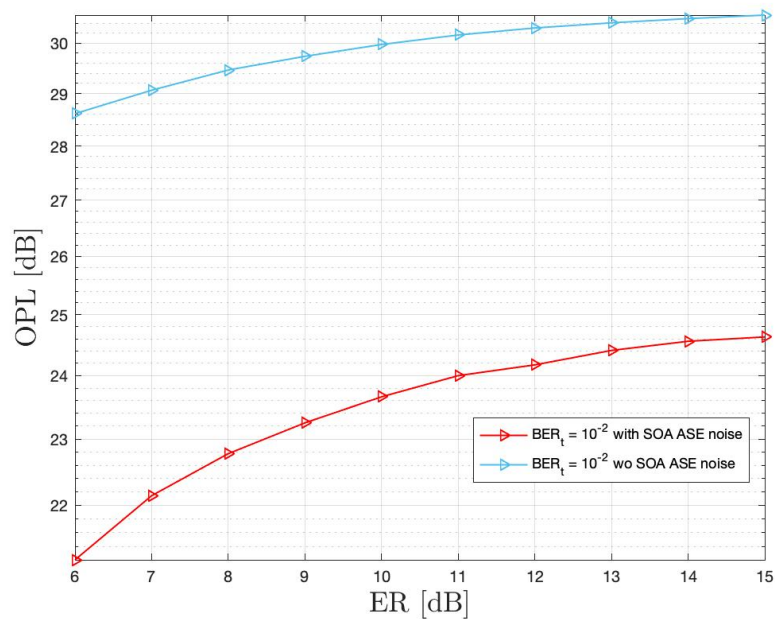


Figure 4.10: ER vs OPL curve with and without ase noise for PAM-4

We observe that the effect of ASE noise is more severe in PAM-4 than in NRZ because more levels are affected in PAM-4. Moreover, the penalty due to ASE noise becomes larger at lower values of extinction ratios due to the fact that the separation between the level is smaller.

Threshold optimization

In Fig. 4.11 we illustrate the results of evaluating Optical Path Loss versus extinction ratio at BER_t of 10^{-2} and BER_t of 10^{-3} : with and without threshold optimization in an ASE noise-limited regime.

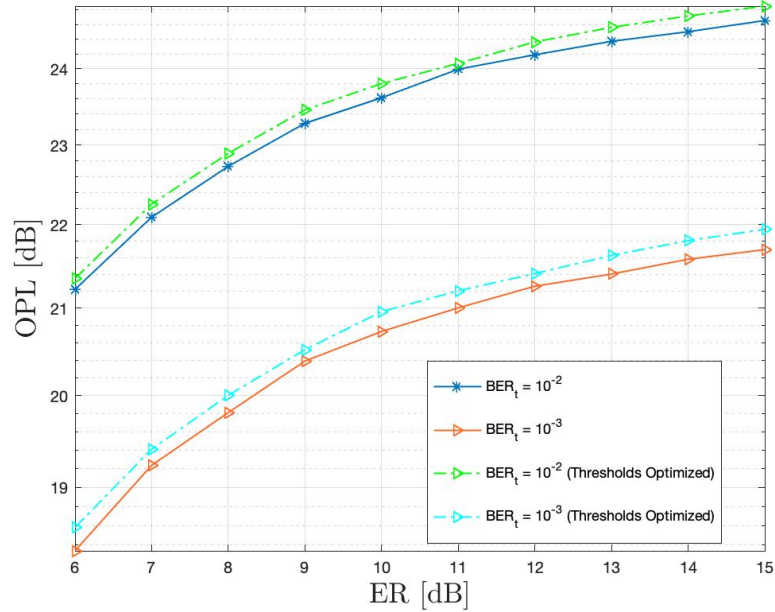


Figure 4.11: ER vs OPL curve with and without threshold optimization for PAM-4 at nominal inner levels

Since ASE noise variance does not depend on the instantaneous received power the noise variance remains constant for all values of extinction ratios in range: what changes is the ratio between ASE to thermal noise. In addition, we notice negligible gain in terms of OPL at BER_t of 10^{-2} and also at BER_t of 10^{-3} . Unlike NRZ, that is due to the fact that, for a PAM-4 at the nominal levels, the threshold optimizer has less dynamic range. In Tab. 4.9 the sensitivity enhancements for PAM-4 are reported at 15 dB of ER:

$BER_t = 10^{-2}$	0.2 dB
$BER_t = 10^{-3}$	0.3 dB

Table 4.9: SOA+PIN sensitivity enhancement for PAM-4 after optimizing thresholds

Thresholds and levels optimization

using the grid-search-based approach we picked up the values for inner levels for SOA+PIN-RX reported in Tab. 2.3.

We illustrate the results of evaluating Optical Path Loss versus Extinction ratio at BER_t of 10^{-2} and BER_t of 10^{-3} with and without optimization.

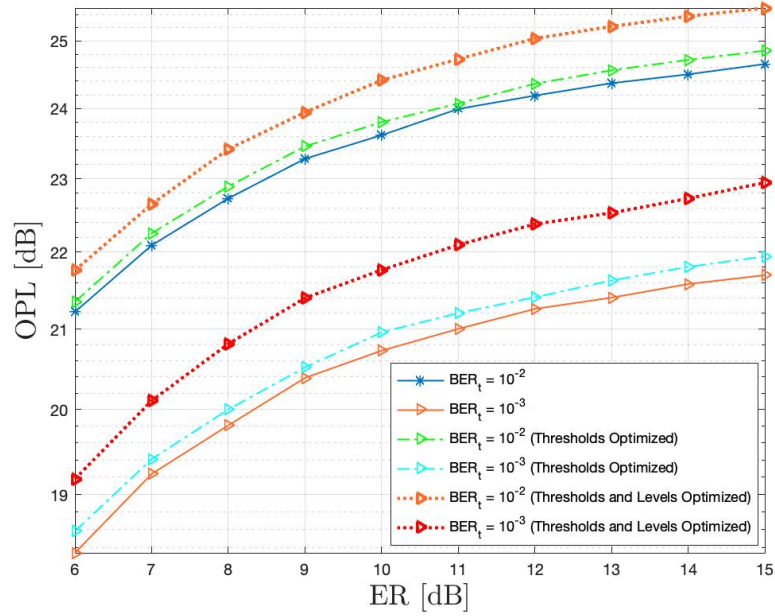


Figure 4.12: ER vs OPL curve with and without threshold optimization relevant to PAM-4 at optimized inner levels

We can notice that the optimization of the inner levels jointly with thresholds show a significant improvement in terms of OPL for SOA+PIN receiver for all extinction ratios, with a behaviour similar to that observed for NRZ, the highest gain is achieved at ER of 15 dB and it is not constant for all values of extinction ratios. The gains in terms of OPL are reported in Tab. 4.10 :

$BER_t = 10^{-2}$	0.8 dB
$BER_t = 10^{-3}$	1.3 dB

Table 4.10: SOA+PIN sensitivity improvement for PAM-4 after optimizing levels and thresholds

4.3.2 Assessment against 3-dB bandwidth of transmitter

In Fig. 4.13 we show the penalties at BER_t of 10^{-2} due to ASE noise in different $f_{3dB,electrical}$ window of 25% of baud rate to 70% (35 GHz) while fixing ER at 9 dB,

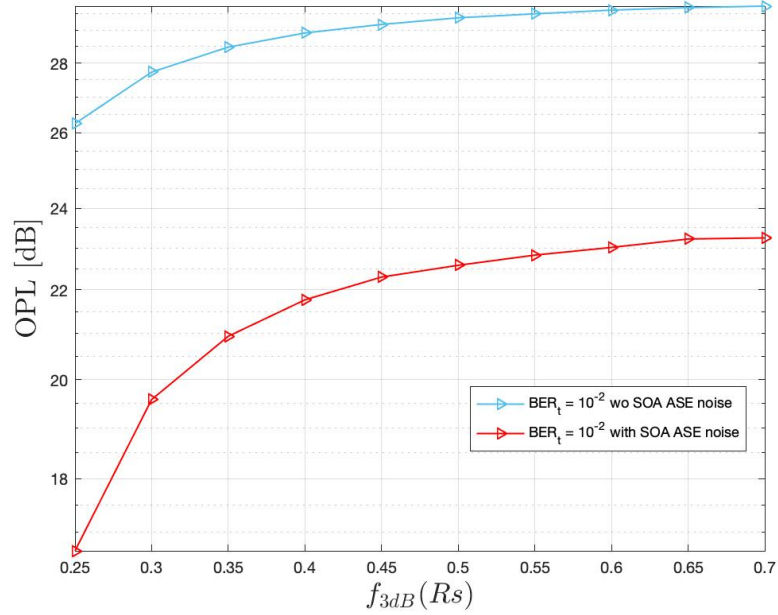


Figure 4.13: $f_{3dB,electrical}$ vs OPL curve with and without ASE noise for PAM-4

We can observe at transmitter cut-off frequency of 25% of baud rate that ASE noise introduces a huge penalty compared to the case of not having ase noise, that is, even while having a FFE implemented. the penalty due to bandwidth limitations at BER of 10^{-2} is reported in 4.11

$$\overline{BER_t = 10^{-2} \quad 5.0 \text{ dB}}$$

Table 4.11: Bandwidth limitation penalty at $f_{3dB,electrical}$ of 25% of baud rate compared to 70% for PAM-4 while having ase noise

Threshold optimization

In Fig. 4.14, we show the effectiveness of performing threshold optimization for different values of $f_{3dB,electrical}$ by evaluating the Optical Path Loss versus 3-dB bandwidth of transmitter normalized by the baud-rate at BER_t of 10^{-2} and at BER_t of 10^{-3} .

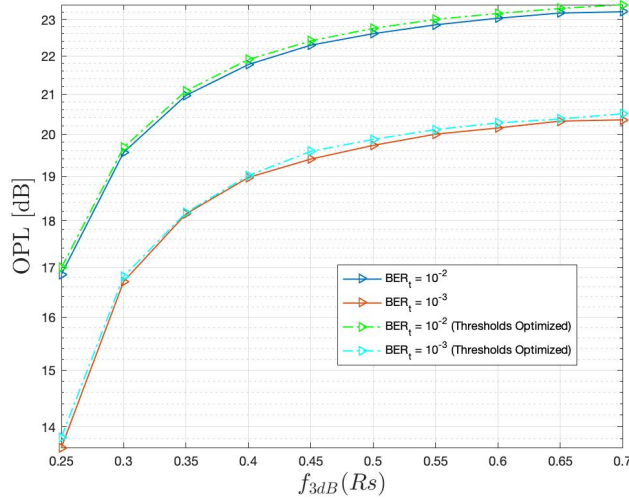


Figure 4.14: $f_{3dB,electrical}$ vs OPL curve with and without threshold and levels optimization relevant to PAM-4 at ER of 9 dB

Remarkably, we have negligible improvements in terms of sensitivity (OPL) at BER_t of 10^{-2} and BER_t of 10^{-3} after optimizing thresholds. they get even worse as we introduce higher bandwidth limitations. the reason behind is that the FFE averages the noise asymmetry out as it tries to minimize ISI by correlating a large number of consecutive symbols with an impulse response. The maximum possible enhancements as we optimize the thresholds only are observed at ($f_{3db} > 0.5 R_s$) and are reported in Tab.4.12:

$BER_t = 10^{-2}$	0.2 dB
$BER_t = 10^{-3}$	0.21 dB

Table 4.12: SOA+PIN sensitivity enhancement for PAM-4

Thresholds and levels optimization

As optimizing the thresholds was found to be negligible, we will proceed with levels and thresholds joint optimization. The inner levels we used are reported in Tab. 2.3.

In Fig. 4.15 we illustrate the results of evaluating Optical Path Loss versus 3-dB bandwidth normalized by the baud-rate at BER_t of 10^{-2} and BER_t of 10^{-3} :with and without optimization

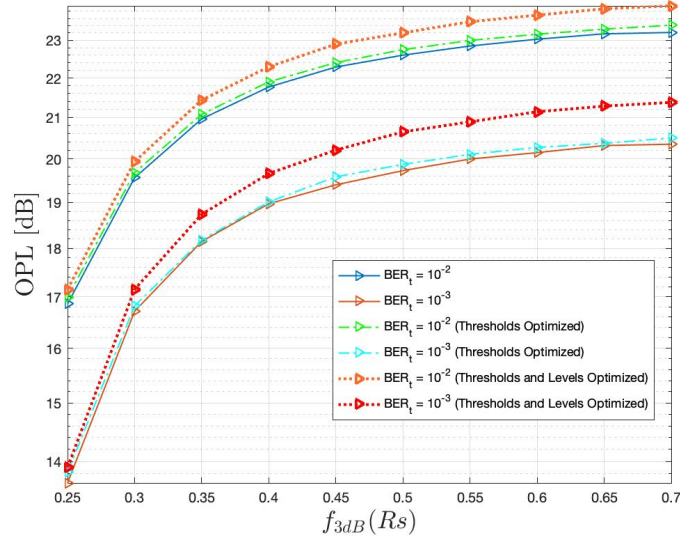


Figure 4.15: $f_{3dB,electrical}$ vs OPL curve with and without threshold and levels optimization relevant to PAM-4 at ER of 9 dB

Again, the major optimization that enhances the overall performance is for the inner levels of the PAM-4. However, the gain totally fades out at $f_{3dB} < 35\%$ of baud rate. that is due to the central limit theorem. As the FFE equalizer takes a large number of samples to compensate for ISI and correlates it with a given impulse response. the variance of the decision variables after equalization will approximately be symmetric. hence, optimization would be useless.

$BER_t = 10^{-2}$	0.5 dB
$BER_t = 10^{-3}$	1.1 dB

Table 4.13: SOA+PIN maximum sensitivity enhancement

4.3.3 Assessment against optical amplifier gain

Similar to what we had done in PAM-2 section, In Fig. 4.16 we show the results of evaluating Optical Path Loss versus SOA gain at BER_t of 10^{-3} : with and without optimization. (while fixing ER at 9 dB, $f_{3dB,electrical}$ at 35 GHz, $f_{3dB,optical}$ at 300 GHz).

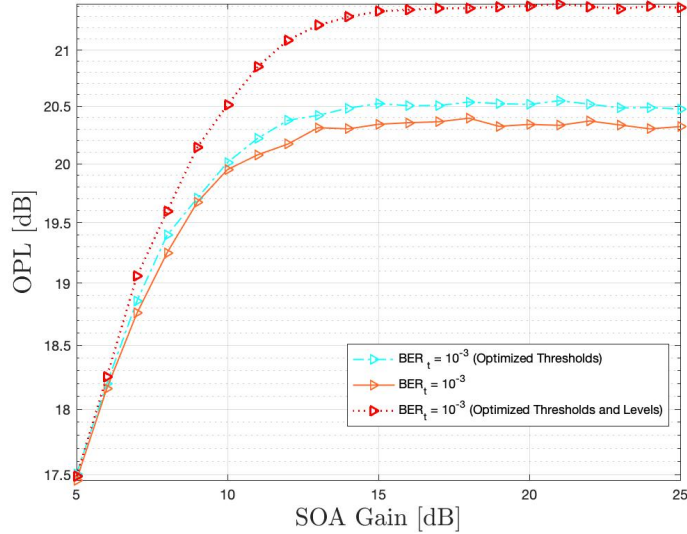


Figure 4.16: SOA gain vs OPL curve with and without threshold optimization for PAM-4

We can see a linear region at gains from 5 to 10 dB where threshold optimization was found to be negligible while there was a remarkable gain in the same region for optimizing the inner levels. the curve then starts being non linear before it moves into saturation. this behaviour due to the fact that, ASE noise dominates thermal noise in the saturation region while at lower gains ASE noise becomes negligible. The sensitivity improvement in the saturation region at BER of 10^{-3} is reported in Tab. 4.14

$BER_t = 10^{-3}$	0.2 dB	Thresholds only
$BER_t = 10^{-3}$	1.1 dB	Thresholds and levels

Table 4.14: SOA+PIN sensitivity enhancement at 25 dB of SOA gain for PAM-4

4.3.4 Assessment against 3-dB bandwidth of optical filter

In Fig. 4.8 we show the sensitivity with and without optimization in a cut off frequency window of 50 to 500 GHz while having $f_{3dB,electrical}$ of 35 GHz, ER of 9 dB and SOA gain of 15 dB.

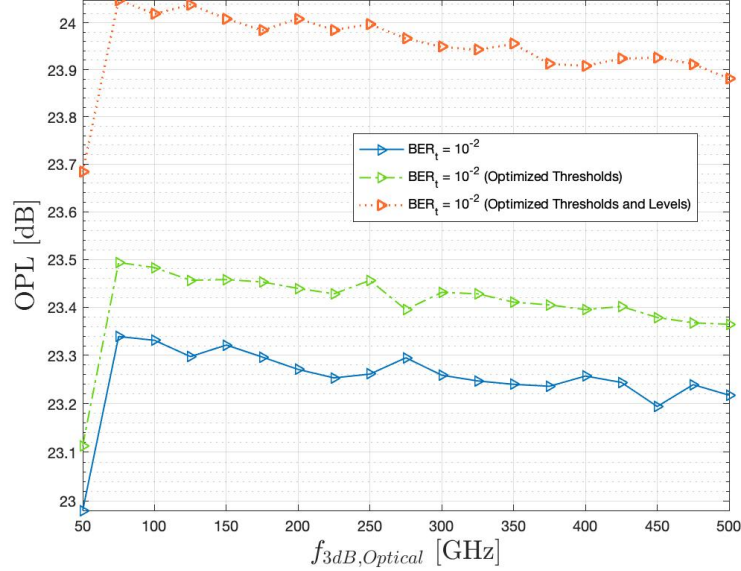


Figure 4.17: $f_{3dB,optical}$ vs OPL curve with and without threshold optimization relevant to PAM-4

Remarkably, as our optical filter band-width gets larger than twice the bandwidth of the shaping filter, it allows more ASE to pass through. thus, system performance is degraded. Also, as we optimize the thresholds only we have a negligible gain while the most significant improvement is a result of optimizing thresholds and levels jointly. The gains in terms of OPL in the region beyond 70 GHz at BER of 10^{-3} are reported in Tab. 4.15

$BER_t = 10^{-3}$	0.2 dB	Thresholds only
$BER_t = 10^{-3}$	1.1 dB	Thresholds and levels

Table 4.15: SOA+PIN sensitivity enhancement at $f_{3dB,optical}$ of 300 GHz for PAM-4

4.4 Conclusions

In this chapter, we simulated SOA+PIN receiver while exploiting a feed-forward equalizer and several optimization techniques.

By looking at the results reported in this chapter, several aspects emerge:

- SOA ASE noise becomes more significant while transmitting
- ASE noise becomes more significant while transmitting a PAM-4 than while transmitting a NRZ at the same baudrate due to the fact that more levels are affected.
- Since ASE noise variance is not dependent on the instantaneous received optical power: optimization of thresholds shows a gain in terms of OPL at higher extinction ratios.
- Optimizing PAM-2 threshold in APD-RX shows a considerable gain which is quite similar to APD. Whereas, thresholds optimization for PAM-4 is negligible.
- By introducing huge bandwidth limitations, the analog signal becomes more vulnerable to distortion due to ISI and as the signal gets digitized and processed by the FFE, this noise asymmetry is averaged out because the FFE considers large number of several consecutive symbols to combat ISI: by correlating them with a given impulse response.
- The optimization of PAM-4 inner levels jointly with thresholds shows a significant sensitivity improvement compared to thresholds only.
- Since ASE noise variance exhibits dependency on SOA gain, the optimization is found to be useful only while operating in ASE noise limited regime.

In the next Chapter, we will introduce topics related to pre-equalization for PAM-4 levels and some final conclusions.

Bibliography

- [1] *History of Information*. URL: <https://www.ciscopress.com/articles/article.asp?p=170740> (cit. on p. 2).
- [2] *Optical Semaphore telegraph*. URL: <https://www.amusingplanet.com/2019/03/the-worlds-first-cyber-attack-happened.html> (cit. on p. 2).
- [3] Z. Ghassemlooy, W. Popoola, and S. Rajbhandari. *Optical Wireless Communications: System and Channel Modelling with MATLAB, Second Edition*. CRC Press, 2019. ISBN: 9781498742702 (cit. on pp. 3, 11, 14).
- [4] *5G fronthaul*. URL: <https://www.viavisolutions.com/en-us/fronthaul> (cit. on p. 4).
- [5] *Passive Optical Network*. URL: <https://www.viavisolutions.com/en-us/passive-optical-network-pon> (cit. on p. 4).
- [6] *Passive Optical Networks Standards*. URL: https://www.researchgate.net/figure/Passive-optical-network-PON-standards_tbl4_335857140 (cit. on p. 6).
- [7] Giorgio Taricco. *INFORMATION AND COMMUNICATION THEORY lecture notes* (cit. on p. 7).
- [8] Tsuyoshi Yamamoto. *High-speed directly modulated lasers*. 2012 (cit. on p. 7).
- [9] T P Lee. *Photodetectors for Optical Fiber Communications EE 233 Seminar*. 1997. URL: https://inst.eecs.berkeley.edu/~ee233/sp06/lectures/Photo_Receiver.pdf (cit. on pp. 9–11).
- [10] *Semiconductor Optical Amplifier*. URL: https://www.rp-photonics.com/optical_amplifiers.html (cit. on p. 13).
- [11] *SOA noise figure*. URL: <https://www.hindawi.com/journals/aot/2017/9053582/> (cit. on p. 13).
- [12] *SOA characteristics*. URL: <https://www.fiber-optic-solutions.com/introduction-semiconductor-optical-amplifier-soa.html> (cit. on p. 13).

- [13] M.J. Connelly. *Semiconductor Optical Amplifiers*. Springer US, 2002. ISBN: 9780792376576 (cit. on p. 13).
- [14] *SOA FPLA and TWSLA*. URL: https://electronics-club.com/semiconductor-optical-amplifiers-soa/#Semiconductor_Optical_Amplifiers_SOA (cit. on p. 13).
- [15] F.P. Miller, A.F. Vandome, and M.B. John. *Gaussian Filter*. 2010. URL: <https://books.google.it/books?id=GUtHYgEACAAJ> (cit. on p. 17).
- [16] Leonardo MINELLI. «Neural networks for optical links nonlinear equalization». M. Eng. thesis. Torino, Italy: Politecnico di Torino, Oct. 2021 (cit. on p. 23).
- [17] ITU-T G.9804 Series of Recs. *50-Gigabit-capable passive optical networks (50G-PON): Physical media dependent (PMD) layer specification*. G.9804.3 (50G-PON PMD). 2021 (cit. on p. 23).
- [18] E. Walach and B. Widrow. «The least mean fourth (LMF) adaptive algorithm and its family». In: *IEEE Transactions on Information Theory* 30.2 (1984), pp. 275–283. DOI: [10.1109/TIT.1984.1056886](https://doi.org/10.1109/TIT.1984.1056886) (cit. on p. 24).
- [19] Andrea Carena. *Computer aided design of communication systems lecture notes* (cit. on p. 24).
- [20] Pablo Torres-Ferrera, Haoyi Wang, Valter Ferrero, and Roberto Gaudino. «100 Gbps/ λ PON downstream O- And C-band alternatives using direct-detection and linear-impairment equalization [Invited]». In: *Journal of Optical Communications and Networking* 13 (2 Feb. 2021), A111–A123. ISSN: 19430639. DOI: [10.1364/JOCN.402437](https://doi.org/10.1364/JOCN.402437) (cit. on pp. 36, 52).